Doctoral Thesis

Development of a Reaction Mechanism for Dual Fuel Combustion Simulations

carried out for the purpose of obtaining the academic degree

Doctor technicae (Dr. techn.)

submitted at TU Wien, Faculty of Mechanical and Industrial Engineering

DI Sebastian Schuh, BSc

Mat.Nr.: 0530580

under the supervision of

Ao. Univ. Prof. DI Dr. Franz Winter

Institute of Chemical, Environmental and Bioscience Engineering

Reviewed by

Univ.-Prof. Dr.-Ing. Michael Wensing
Department of Chemical and Biological Engineering
Friedrich-Alexander-Universität Erlangen-Nürnberg
Am Weichselgarten 8
91058 Erlangen
Germany

Univ.-Prof. DI Dr.-Ing. Markus Lehner
Chair of Process Technology and Industrial Environmental Protection
Montanuniversität Leoben
Franz-Josef-Straße 18
8700 Leoben
Austria

This work was supported by the Austrian Research Promotion Agency (FFG) within the framework of the project “Dual Flame” (grant number 850690).

I confirm, that going to press of this thesis needs the confirmation of the examination committee.

Affidavit

I declare in lieu of oath, that I wrote this thesis and performed the associated research myself, using only literature cited in this volume. If text passages from sources are used literally, they are marked as such.

I confirm that this work is original and has not been submitted elsewhere for any examination, nor is it currently under consideration for a thesis elsewhere.

Vienna, May, 2020

_____

Signature

Abbreviations

CFD	Computational fluid dynamics
CN	Cetane number
CV	Combustion vessel
FAU	Friedrich-Alexander-Universität Erlangen-Nürnberg
IDT	Ignition delay time
LLNL	Lawrence Livermore National Laboratory
MN	Methane number
NIST	National Institute of Standards and Technology
NTC	Negative temperature coefficient
PCFC	Physico chemical fundamentals of combustion
RCEM	Rapid compression expansion machine
RCM	Rapid compression machine
ST	Shock tube
TDC	Top dead center
UV	Ultraviolet
MZ	Methanzahl
VB	Verbrennungsbombe
ZVZ	Zündverzugszeit
A	Pre-exponential factor
β	Temperature exponent
C_{pk}^0	Standard state molar heat capacity at constant pressure of the kth species
E_A	Activation energy
ϕ	Fuel-air equivalence ratio
H_k^0	Standard state molar enthalpy of the kth species
k	Reaction rate coefficient
p	Pressure
R	Universal gas constant
S_k^0	Standard state molar entropy of the kth species
T	Temperature

Acknowledgements

An dieser Stelle möchte ich mich bei allen Menschen bedanken, die mich im Rahmen meines Doktoratsstudiums sowohl aktiv als auch passiv unterstützt haben.

Ein besonderer Dank geht an Prof. Franz Winter, der mir die Möglichkeit gab, diese Doktorarbeit durchzuführen, für seine Betreuung und Unterstützung über die Jahre sowie die angenehme Arbeitsatmosphäre.

Außerdem möchte ich mich bei meinen Kollegen an der TU Wien bedanken, insbesondere bei Jens Frühhaber, die mich im Verlauf meines Studiums mit produktiven Gesprächen begleitet haben.

Einen Dank möchte ich auch den Kollegen an der RWTH Aachen für die gute Zusammenarbeit aussprechen.

Des Weiteren möchte ich mich für die Begutachtung der Arbeit bei Prof. Michael Wensing und Prof. Markus Lehner bedanken.

Ebenso bedanken möchte ich mich bei meinen Kollegen an der Fachhochschule Burgenland und Forschung Burgenland. Die Tatsache, dass ich bei der Durchführung meiner Doktorarbeit stets unterstützt wurde, sei es durch ein flexibles Zeitmanagement innerhalb von Projekten oder der problemlosen Gewährung meiner Bildungskarenz, weiß ich sehr zu schätzen.

Bedanken möchte ich mich auch bei der Firma LOGE AB für die Zurverfügungstellung der Simulationssoftware LOGEresearch sowie für die persönliche Beratung, im Speziellen durch Lars Seidel.

Bei dieser Gelegenheit gilt es auch der österreichischen Forschungsförderungsgesellschaft FFG meinen Dank für die finanzielle Unterstützung des Projektes auszusprechen, in Rahmen dessen die Forschungsarbeiten für diese Dissertation durchgeführt wurden.

Am Schluss möchte ich einen sehr großen Dank meiner Familie und meinen Freunden aussprechen. Im Speziellen möchte ich hierbei meinen Eltern Ulrike und Gerhard, meiner Frau Andrea und meinem Sohn Tim danken. Sie hielten mir stets den Rücken frei, um mich auf die Arbeit konzentrieren zu können – akzeptierten, dass Papa manchmal nicht so viel Zeit zum Spielen hatte – schenkten mir immer ein offenes Ohr – gaben mir die notwendige Ruhe, Sicherheit und Kraft für die Erstellung dieser Doktorarbeit.

Abstract

The limitation of anthropogenic global warming will most likely prove to be one of the greatest challenges in human history. In the 2015 Paris Climate Agreement, nations agreed to take measures to limit worldwide warming to 2°C. A significant reduction in greenhouse gases is required to achieve this target. While the electrification of different modes of transport can play an important role in achieving this goal, the optimization of existing and development of new, more efficient conventional combustion technologies can also provide an important contribution. In the transport sector, for example, the use of dual fuel engines instead of pure diesel engines offers potential for emission savings. In the dual fuel combustion process, a mixture of air and fuel gas is compressed and ignited by the injection of a reactive liquid fuel pilot, such as diesel.

In the development of modern combustion engines, the use of simulations has become indispensable. One prerequisite for simulating the engine process is the availability of a reaction mechanism for calculating the chemical reactions taking place during ignition and combustion. The dual fuel combustion process, in which two different fuel types interact, is very complex and not yet understood in detail.

This thesis aims to analyze the dual fuel combustion process in detail and develop a reaction mechanism for the simulation of this process. The ignition delay times (IDTs) of homogeneous mixtures of methane, propane and *n*-heptane, determined with a rapid compression machine (RCM) and a shock tube (ST), were used to verify the simulation results. The tests were performed at pressures of 60 to 100 bar, temperatures of 671 to 1284 K and a fuel-air equivalence ratio between 0.526 and 0.816. With IDTs between 0.06 and 92 ms, nearly three orders of magnitude were spanned. The experimental investigation on inhomogeneous mixtures was performed with a rapid compression expansion machine (RCEM) and a combustion vessel (CV) by injecting a diesel jet into air (RCEM and CV tests) or a natural gas-air mixture (RCEM tests). In the CV, the pressure was 60 bar at a temperature between 823 and 973 K. The chamber pressure at the start of diesel injection in the RCEM measured over 60 bar.

The Complete San Diego mechanism with a heptane extension served as the basis for the mechanism development. Despite its compactness, it delivered the most promising results of all potential mechanisms examined over the entire parameter range.

Sensitivity and flow analyses were performed to identify the reactions that could be used for the optimization of the reaction mechanism. The mechanism was adapted by adjusting the corresponding Arrhenius parameters and the associated change in reaction rate coefficients.

The TU Wien dual fuel mechanism optimized for RCEM and CV-CFD simulations, which consists of 301 reactions and considers 64 species, can reproduce the IDTs determined in the RCEM both in pure diesel operation and in dual fuel operation. Comparisons with the values measured in the CV show a partly significant improvement of the simulated ITDs in the sense of an approximation to the experimental values in the considered temperature range from 823 to 973 K. The ignition characteristic of gas mixtures of methane and propane can be reproduced correctly in a methane number (MN) range from 70 to 100.

During the further development of the reaction mechanism, intended to discover a greater range of applications, the purely kinetic-controlled ignition process was investigated in homogeneous mixtures. A major advantage of dual fuel operation over pure diesel operation is the significantly reduced emission of nitrogen oxides (NO_x). To calculate the formation of NO_x during combustion, the reaction mechanism was extended to include 344 reactions and consider 75 species. One goal of the ongoing development process of the mechanism was to improve the calculation of the ignition properties of methane-propane mixtures. Thus, the MN range with satisfactory IDT calculation could be extended from 70 to 100 to the entire examined range of 50 to 100.

This thesis also examined the simulation of flame propagation in the background gas of the combustion chamber. Experimentally determined flame speeds from the literature at pressures of about 10 to 20 bar, temperatures between 300 and 400 K and a fuel-air equivalence ratio of 0.7 to 1.4 of methane-air mixtures were used to evaluate the simulated data. Through sensitivity analyses, influential reactions were identified and used to optimize the mechanism. The mechanism

adjustment allows the flame speed to be reproduced well over the mentioned parameter range. In addition to the optimized calculation of the ignition properties of methane-propane mixtures, the TU Wien dual fuel mechanism 2.0 shows an improved reproduction of the measured IDT values of the methane-*n*-heptane and methane-propane-*n*-heptane mixtures investigated and thus exceeds the results from all other mechanisms previously considered. The developed reaction mechanisms offer the scientific community new possibilities for more in-depth research in the field of dual fuel combustion.

Kurzfassung

Eine der wohl größten Herausforderungen in der Menschheitsgeschichte stellt die Begrenzung der vom Mensch verursachten globalen Erwärmung dar. Im Pariser Klimaabkommen wurde festgehalten, dass Maßnahmen getroffen werden müssen, um die Erwärmung auf 2°C einzugrenzen. Um dies zu erreichen, ist eine deutliche Reduktion der Treibhausgase erforderlich. Die Elektrifizierung im Mobilitätssektor spielt eine wichtige Rolle bei der Erreichung dieses Ziels, aber auch im Bereich der konventionellen Verbrennungstechnik können die Optimierung bestehender und die Entwicklung neuer hocheffizienter Technologien einen wichtigen Beitrag leisten. Im Verkehrssektor bietet beispielsweise der Einsatz von Dual Fuel-Motoren anstelle von reinen Dieselmotoren das Potenzial für Emissionseinsparungen. Beim Dual Fuel-Verbrennungsprozess wird ein Gemisch aus Luft und Brenngas verdichtet und durch die Einspritzung eines reaktiven flüssigen Treibstoff-Piloten, wie beispielsweise Diesel, gezündet.

Bei der Entwicklung von modernen Verbrennungsmotoren ist der Einsatz von Simulationen zu einem mittlerweile unverzichtbaren Instrument geworden. Um den Motorprozess simulieren zu können, ist eine Voraussetzung die Verfügbarkeit eines Reaktionsmechanismus zur Berechnung der bei der Zündung und Verbrennung ablaufenden chemischen Reaktionen. Der Dual Fuel Verbrennungsprozess, in dem zwei verschiedenen Kraftstoffarten interagieren, ist sehr komplex und noch nicht im Detail verstanden.

Ziel dieser Arbeit war es den Dual Fuel Verbrennungsprozess genauer zu analysieren und einen Reaktionsmechanismus für die Simulation dieses Prozesses zu entwickeln. Zur Verifizierung der Simulationsergebnisse dienten die mit einer Rapid Compression Maschine (RCM) und einer Shock Tube (ST) ermittelten Zündverzugszeiten (ZVZs) homogener Gemische aus Methan, Propan und *n*-Heptan, welche bei Drücken von 60 bis 100 bar, Temperaturen von 671 bis 1284 K und einem Brennstoff-Luft-Äquivalenzverhältnissen zwischen 0,526 und 0,816 durchgeführt wurden. Mit ZVZs von 0,06 bis 92 ms wurden dabei knapp drei Größenordnungen überspannt. Die experimentelle Untersuchung inhomogener Gemische erfolgte mit einer Rapid Compression Expansion Machine (RCEM) und einer Verbrennungsbombe (VB) durch Einspritzung eines Dieselstrahls in Luft bzw. ein Erdgas-Luft-Gemisch. In der VB lag der Druck bei 60 bar im Temperaturbereich 823 bis 973 K. Der Kammerdruck bei Einspritzungsbeginn von Diesel in der RCEM lag bei über 60 bar.

Als Basis der Mechanismusentwicklung diente der Complete San Diego Mechanismus mit Heptan-Erweiterung, der trotz seiner Kompaktheit über den gesamten untersuchten Parameterbereich betrachtet die vielversprechendsten Ergebnisse von allen untersuchten Mechanismen lieferte.

Zur Identifizierung jener Reaktionen, die für die Optimierung des Reaktionsmechanismus herangezogen werden konnten, wurden Sensitivitäts- und Flussanalysen durchgeführt. Die Adjustierung des Mechanismus erfolgte durch Anpassung der entsprechenden Arrheniusparameter und der damit verbundenen Veränderung der Reaktionsratenkoeffizienten.

Der für die RCEM- und VB-CFD-Simulationen optimierte TU Wien Dual Fuel-Reaktionsmechanismus, bestehend aus 301 Reaktionen unter Berücksichtigung von 64 Spezies, ist in der Lage, die in der RCEM ermittelten ZVZs sowohl im reinen Dieselbetrieb als auch im Dual Fuel-Betrieb zu reproduzieren. Vergleiche mit Messwerten in der VB zeigen eine zum Teil signifikante Verbesserung der simulierten ZVZs im betrachteten Temperaturbereich von 823 bis 973 K im Sinne einer Annäherung an die experimentellen Werte. Die Zündcharakteristik von Gasgemischen aus Methan und Propan kann in einem Methanzahl (MZ)-Bereich von 70 bis 100 korrekt wiedergegeben werden.

Bei der Weiterentwicklung des Reaktionsmechanismus mit der Absicht ein breiteres Anwendungsspektrum zu erhalten, wurde der rein Kinetik-kontrollierte Zündvorgang durch die Untersuchung homogener Gemische betrachtet. Ein wesentlicher Vorteil des Dual Fuel-Betriebs gegenüber dem reinen Dieselbetrieb ist die deutlich reduzierte Emission von Stickoxiden (NO_x). Um die Bildung von NO_x bei der Verbrennung berechnen zu können, wurde der Reaktionsmechanismus erweitert und umfasste fortan 344 Reaktionen unter Berücksichtigung von 75 Spezies. Ein Ziel im Entwicklungsprozess des Mechanismus war es, die Berechnung der Zündeigenschaften von Methan-

Propan-Gemischen zu verbessern. So konnte der MZ-Bereich mit zufriedenstellender ZVZ-Berechnung von 70 bis 100 auf den gesamten experimentell untersuchten Bereich von 50 bis 100 erweitert werden.

Ein weiteres Thema war die Simulation der Flammenausbreitung im Hintergrundgas der Brennkammer. Zur Bewertung der simulierten Daten dienten experimentell ermittelte Flammengeschwindigkeiten aus der Literatur bei Drücken von etwa 10 bis 20 bar, Temperaturen zwischen 300 und 400 K und einem Brennstoff-Luft-Äquivalentverhältnis von 0,7 bis 1,4 von Methan-Luft-Gemischen. Mit Hilfe von Sensitivitätsanalysen wurden einflussreiche Reaktionen identifiziert und für die Optimierung des Mechanismus herangezogen. Durch Anpassung des Mechanismus ist es möglich, die Flammengeschwindigkeit über den genannten Parameterbereich gut zu reproduzieren. Neben der optimierten Berechnung der Zündeigenschaften von Methan-Propan-Gemischen zeigt der TU Wien Dual Fuel Mechanismus 2.0 eine verbesserte Reproduktion der Messwerte der untersuchten Methan-*n*-Heptan- und Methan-Propan-*n*-Heptan-Gemische und übertrifft damit die Ergebnisse aller zuvor betrachteten Mechanismen. Die entwickelten Reaktionsmechanismen bieten der wissenschaftlichen Gemeinschaft neue Möglichkeiten zur detaillierten Erforschung des Dual Fuel Verbrennungsprozesses.

List of Papers included in the Thesis

Schuh, S.; Ramalingam, A.K.; Minwegen, H.; Heufer, K.A.; Winter, F. Experimental Investigation and Benchmark Study of Oxidation of Methane–Propane–n-Heptane Mixtures at Pressures up to 100 bar. Energies 2019, 12, doi:10.3390/en12183410.

Schuh, S.; Frühhaber, J.; Lauer, T.; Winter, F. A Novel Dual Fuel Reaction Mechanism for Ignition in Natural Gas–Diesel Combustion. Energies 2019, 12, doi:10.3390/en12224396.

Schuh, S.; Winter, F. Dual Fuel Reaction Mechanism 2.0 including NOx Formation and Laminar Flame Speed Calculations Using Methane/Propane/n-Heptane Fuel Blends. Energies 2020, 13, doi:10.3390/en13040778.

List of Papers not included in the Thesis

Frühhaber, J.; Peter, A.; Schuh, S.; Lauer, T.; Wensing, M.; Winter, F.; Priesching, P.; Pachler, K. Modeling the Pilot Injection and the Ignition Process of a Dual Fuel Injector with Experimental Data from a Combustion Chamber Using Detailed Reaction Kinetics. 2018, SAE Technical Paper 2018-01-1724, doi:10.4271/2018-01-1724.

Conference Contributions

Schuh, S.; Winter, F. Comparing the Influence of Propane and n-Heptane Addition on Methane Ignition. 8th European Combustion Meeting, Dubrovnik, Croatia, 2017.

Schuh, S.; Winter, F. Simulation der Verbrennung in der Gasphase. 9. Österreichisches IEA Wirbelschichttreffen, Bad Blumau, Austria, 2017.

Peter, A.; Frühhaber, J.; Schuh, S.; Lauer, T.; Winter, F.; Priesching, P.; Wensing, M. Flame quenching during dual-fuel operation investigated in experiments and simulation. THIESEL 2018 Conference on Thermo- and Fluid Dynamic Processes in Direct Injection Engines, Valencia, Spain, 2018.

Schuh, S.; Frühhaber, J.; Winter, F. Development of a Mechanism for Dual Fuel Combustion. Joint Meeting of the German and Italian Sections of the Combustion Institute, Sorrento, Italy, 2018.

Schuh, S.; Winter, F. Optimization of a Mechanism for Dual Fuel Combustion [Poster]. 37th International Symposium on Combustion, Dublin, Ireland, 2018.

Schuh, S.; Winter, F. Simulating the flame velocity of methane- and n-heptane-air mixtures with a reaction mechanism for dual fuel combustion and further mechanism optimization by comparison with experimental data. 1st International Conference on Smart Energy Carriers, Naples, Italy, 2019.

Schuh, S.; Winter, F. Laminar flame speed simulations of methane-air and n-heptane-air mixtures by using an adapted mechanism. 9th European Combustion Meeting, Lisbon, Portugal, 2019.

Contents

1 Research Issues

The dual fuel engine possesses a long history. In 1901, Rudolf Diesel received the first patent application for a dual fuel engine [1]. This engine type's name is derived from its use of two different fuels for operation. The basic mode of operation as described over 100 years ago remains relevant today. The combustion chamber is first filled with a mixture of fuel gas and air, which is then compressed by the upward movement of the engine piston. The temperature and pressure achieved in this process are not sufficient to cause auto ignition of the fuel gas-air mixture. Rather, only an injection of a second fuel component with a higher reactivity and lower ignition threshold can induce the ignition and combustion of the fuel components. Figure 1 demonstrates a schematic representation of the steps in this process.

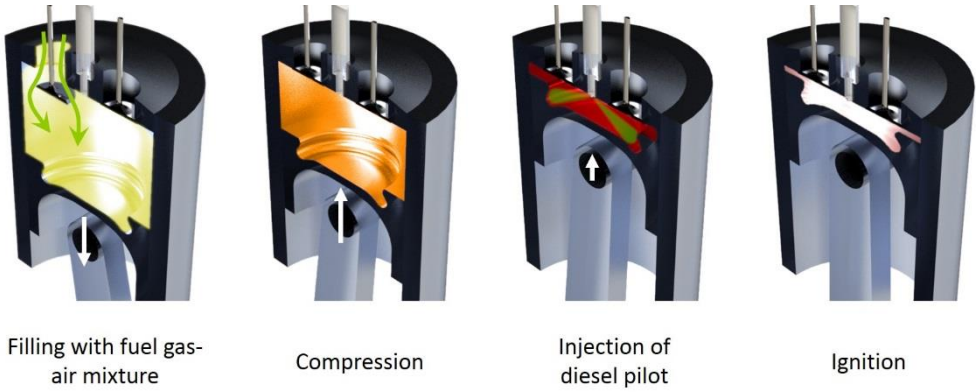

Figure 1. Schematic representation of the dual fuel combustion process from filling the combustion chamber with a fuel gas-air mixture to ignition.

Specifically, an engine in this operating mode is designated as a premixed dual fuel engine. Later, more dual fuel engine types were developed, such as high-pressure direct injection gaseous-fueled dual fuel engines [1], which embeds natural gas under high pressure shortly before or after the injection of the fuel component with higher reactivity. However, the following chapters use the term dual fuel engine as a reference to the premixed dual fuel engine.

Historically, dual fuel engine were increasingly used for stationary operation after the end of the Second World War when large quantities of crude oil began to be extracted. In order to ensure the usage of the natural gas resulting from this increased production, the gas was added to the supply air of diesel engines and co-combusted [2]. However, unlike pure diesel engines, the dual fuel engine did not flourish, as it requires a more complex fuel supply and control system. Thus, due to the low oil prices and the associated low diesel price until the end of the 1960s and in the 1990s [3], no economic incentive to change to dual fuel engines existed. The rise in oil prices in the last two decades and the simultaneous availability of cheap natural gas changed this situation and increased the relative cost-effectiveness of using dual fuel engines.

Stricter laws on exhaust gas emissions have introduced an even more important reason for the growing interest in dual fuel engines. The Paris Climate Change Convention required its signatories to drastically reduce their greenhouse gas emissions to keep global warming below 2°C [4]. In addition to carbon dioxide (CO_2) emissions, the high concentration of nitrogen oxides (NO_x) in the exhaust gas of diesel engines also represents a major environmental and health problem. As an example, the large diesel engines used in shipping account for about 15 % of total global NO_x emissions [5]. The stricter regulations in the shipping sector are intended to greatly reduce NO_x emissions due to their irritating and damaging effect on respiratory organs [6]. While a maximum NO_x emission of 17 g/kWh was permitted until 2010 for ship engines with a speed of less than 130 revolutions per minute by IMO Tier I standards, this limit was reduced to 3.4 g/kWh [7] on 1 January 2016 (IMO Tier III). The regulations have become stricter not only in shipping, but also in freight

transport. The limit on NO_x emissions from heavy commercial vehicles was lowered from 15.8 g/kWh (Euro 0) to 0.4 g/kWh (Euro VI) [8].

To comply with these emission limits with diesel engines, more technical innovation is necessary. The changeover or conversion from diesel engines to dual fuel engines thus represents an attractive option. Compared to diesel engines, dual fuel engines offer the possibility of a significant reduction in CO_2 and especially NO_x emissions [2,9]. To achieve this, as much diesel as possible must be replaced by natural gas.

Seen in this context, the use of pure gas engines could appear preferable at first sight. However, this conclusion fails to consider the numerous advantages that the dual fuel engine offers over the natural gas engine. For example, dual fuel engines can use gases of different quality and origin and tend to knock less. Because dual fuel engines are designed similarly to the robustly constructed diesel engines, they show a high durability and resistance. In addition, the engine can operate over a larger fuel-air equivalence ratio. Nevertheless, the high compression ratios and torque development of the diesel engine can be maintained. Furthermore, due to the presence of two fuel systems, the dual fuel engine offers the possibility of switching to diesel operation in exceptional cases of gaseous fuel shortages, thus avoiding the loss of range. [1]

Today, dual fuel engines are offered by various manufacturers. However, although the dual fuel concept successfully provides significant advantages in terms of exhaust emissions over pure diesel engines, thorough knowledge of the system is required to optimize the engine components and control and thus obtain maximum performance with minimum system emissions.

The dual fuel combustion process itself is extremely complex and not yet fully understood. When diesel is injected into the compressed natural gas-air mixture, the fuel components are inhomogeneously distributed in the combustion chamber. The evaporation of the diesel fuel and the associated cooling can trigger large local temperature gradients. The onset of ignition thus depends on a number of components, such as the pressure and temperature in the different areas of the combustion chamber, the mixing of the natural gas-air mixture with diesel within the diesel spray and the resulting fuel-air equivalence ratio, as well as the mutual interactions and influence of the fuel components on ignition. Depending on the location of ignition, a specific spread of the flame front results, propagating into the natural gas-air background mixture and finally inducing the combustion of all the fuel in the combustion chamber. Since methane may greatly contribute to global warming [10], the entire fuel must be converted during dual fuel combustion for environmental and cost reasons, since a costly exhaust gas treatment is necessary for unburnt components.

Extensive tests on engine test benches are essential to achieve the optimum design of all engine components and the most efficient setting of the engine management system. Due to the high operating costs of such test benches, they contribute a great deal to the overall development costs of the engine. The implementation of parts of this optimization process through simulation, which presupposes the availability of an appropriate reaction mechanism, could result in a reduction of the required engine test bench time.

2 Objective and Structure of the Thesis

The dual fuel combustion process is highly complex. To reconstruct this process by simulation, appropriate theoretical tools are required. This thesis therefore aimed to investigate dual fuel combustion in detail using simulations and to optimize the calculation of the chemical processes that occur during ignition and combustion. To reproduce the working process in the dual fuel engine in detail, the use of computational fluid dynamics (CFD) simulations is essential. As this type of simulation is very computationally intensive, the reaction mechanism used must overcome the following challenges: on one hand, the mechanism simulation must be detailed enough to correctly reflect the necessary aspects of combustion. On the other hand, to keep the computational effort manageable, the mechanism should be kept as small as possible. The thesis thus targeted the development of a mechanism as compact as possible but still capable of reproducing the ignition and combustion process satisfactorily.

As diesel and natural gas consist of a variety of species, simpler substitutes had to be defined to allow feasible simulations in a reasonable time frame. In this thesis, *n*-heptane was used as a diesel surrogate, natural gas was substituted by a mixture of methane and propane.

As part of this thesis, three journal publications were prepared and published. The first paper (hereafter defined as Paper I) discusses experimental measurements of the ignition properties of homogeneous methane-propane-*n*-heptane mixtures using a rapid compression machine (RCM) and a shock tube (ST). The operating conditions of a 1-cylinder dual fuel test engine were considered in choosing the composition and test conditions of the homogeneous mixtures to be investigated. Various *n*-heptane reaction mechanisms studied in the literature were examined to determine to what extent they could reproduce the measured ignition delay times.

The second paper (Paper II) extends the investigation of the *n*-heptane mechanisms. By comparing measured and calculated ignition delay times, the Complete San Diego mechanism with *n*-heptane extension [11] was found to show the highest potential. The paper aimed to use the mechanism for CFD simulations to reproduce measurement data from a rapid compression expansion machine (RCEM) and a combustion vessel (CV). Through flow and sensitivity analyses, the mechanism was evaluated and optimized to such an extent that the experimental results could be reproduced satisfactorily, resulting in a mechanism with a specific field of application.

The mechanism was extended to allow the calculation of the formation of nitrogen oxides during combustion as well as the acquisition of a mechanism that could be used for a wider parameter range. The optimization process focused on the kinetically controlled ignition processes, especially in homogeneous mixtures, to exclude influences on the ignition due to inhomogeneities in the fuel-air mixture caused by diesel spray injection. Furthermore, the propagation of the flame front after ignition was investigated by laminar flame speed simulations. With the help of sensitivity analyses and a further adjustment of the mechanism, the reproduction of the experimental values could be improved. All these investigations and results are discussed in the third paper (Paper III).

3 Materials and Methods

As mentioned in the introduction, the dual fuel combustion process is very complex, due to the disparate physical and chemical properties of both fuels used as well as the different ways in which they are introduced and subsequently distributed within the combustion chamber. Diesel and natural gas comprise the two fuels considered in this thesis.

3.1 Fuels and Surrogates

Diesel is a mixture of hydrocarbons with a carbon number between six and 28, which consists of about 73 % alkanes and 27 % aromatic hydrocarbons [12]. Due to the broad spectrum of species, diesel does not have a defined boiling point but a boiling range that extends from 180 to 360°C [13].

The cetane number (CN) was introduced to specify the ignitability of a diesel fuel. A higher CN indicates a more ignitable fuel. A test engine, which is operated with a mixture consisting of α-methylnaphthalene, whose CN is 0, and n-hexadecane, whose CN is 100, aids in the experimental determination of the CN. To do so, the mixture ratio of α-methylnaphthalene and n-hexadecane is adjusted so that the test engine shows the same operation characteristics as when operated with the fuel under consideration [13].

The second fuel, natural gas, consists of a mixture of light hydrocarbons such as methane, ethane, propane and others, as well as non-combustible gases like carbon dioxide and nitrogen. The exact composition depends on the region in which the natural gas is extracted. The amount of methane, the main component of natural gas, can differ considerably. For example, CIS-H natural gas consist of 98 % methane [14], whereas Khuff gas consists of only 69 % methane [15]. Similar to the CN, a characteristic number for gas mixtures, the methane number (MN), also exists. The MN indicates the knock resistance of the gas or gas mixture and is determined using an experimental engine. The reference gases used are methane with a high knock resistance and a defined MN of 100, and hydrogen, whose MN is defined as 0 [16]. Due to the different compositions of natural gas in different extraction regions [14,15,17,18], the respective MNs also differ. An overview of the MNs of natural gas from different extraction areas calculated with the Westport Fuel Quality Calculator [19] can be seen in Figure 2.

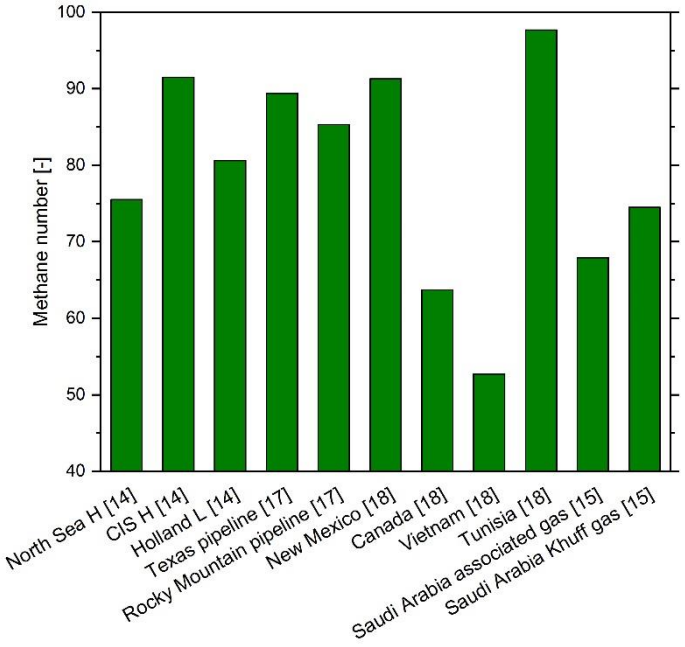

Figure 2. Methane numbers of various natural gases from different extraction areas. [20]

Due to the high number of species in the aforementioned fuels, a simulation of the ignition and combustion process is extremely complex, with unmanageable calculation times. To overcome this

problem, combustion simulations commonly use surrogate fuels [21], which consist of a greatly reduced number of species. This simplification inevitably leads to restrictions on the application of the substitutes. In this respect, when choosing the surrogate fuel, researchers should consider which physical and chemical properties of the original fuel are most important to ensure that the surrogate fuel properly reflects the required characteristics of the fuel substituted for.

n-Heptane, a frequently used substitute in dual fuel investigations [22-24], was chosen as a one-component surrogate for diesel in the investigation of the ignition process. Diesel and *n*-heptane's similarity in ignitability becomes apparent when comparing their CNs. *n*-Heptane possesses a CN of 56 [25]. According to the DIN EN590 standard of October 2009, diesel must have a minimum CN of 51 [26]. The experimental measurement of the ignition delay time at pressures of 60 to 90 bar and a temperature between 550 and 700°C with a combustion vessel from the Friedrich-Alexander-Universität Erlangen-Nürnberg (FAU) [27], confirms the similar ignition properties of diesel (with a verified CN of 52.4) and *n*-heptane as shown in Figure 3, thus legitimizing the use of *n*-heptane as a diesel substitute.

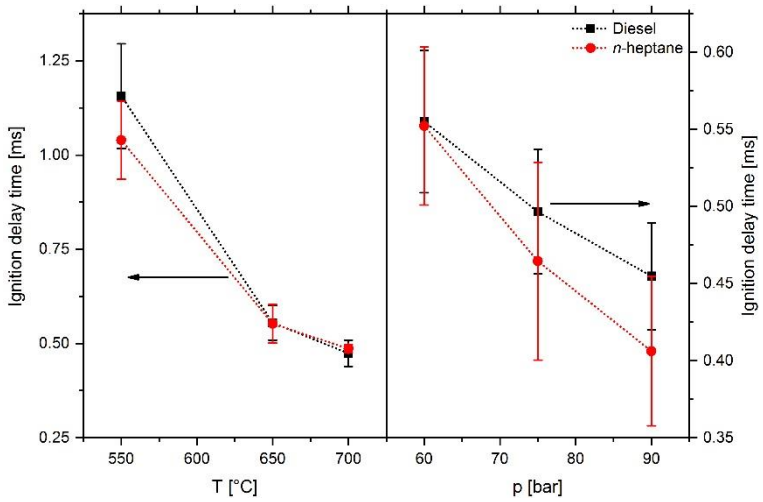

Figure 3. Comparison of measured ignition delay times of diesel and *n*-heptane at a pressure of 60 bar and a variation of the temperature between 550 and 700°C (left) as well as at a temperature of 650°C and a pressure variation between 60 and 90 bar (right).

Like diesel, a surrogate for natural gas must also be found to perform simulations within a reasonable timeframe. Since methane is the main component of natural gas, it is often used as the only substitute fuel [22,24]. By definition, methane possesses an MN of 100 and shows a much higher knock resistance than most natural gases. To better mimic the knock resistance of natural gas, this study used a mixture of methane and propane. Methane and propane comprised 95 mol% and 5 mol% respectively for most of the mixtures. This mixture resulted in a MN of 79.2, slightly higher than the mean value of the MN of the natural gases shown in Figure 2.

3.2 *Oxidation of Hydrocarbons*

In an ideal combustion of hydrocarbons, meaning sufficient oxygen supply and no formation of pollutants such as NO_x, the combustion process induces the formation of CO_2 and water (H_2O). This process takes place exothermically, releasing heat. The resulting products thus demonstrate a more stable and lower total energy balance level than the educts. This statement also holds true for a variety of combustible materials like wood and coal. However, a wooden house obviously does not immediately burst into flames upon contact with the oxygen in the air inducing a more energetically favorable state. This does not occur because energy must first be expended to initiate the combustion process, i.e., an energy barrier must be overcome. Once the reaction has begun, more energy is released than required to overcome the energy barrier; thus, the combustion process maintains itself. The combustion of *n*-heptane (n-C_7H_{16}) serves as a good example of the combustion of hydrocarbons.

n-C_7H_{16} is a linear hydrocarbon composed of seven carbon atoms, connected to each other by single bonds, and 16 hydrogen atoms. To oxidize one mole of *n*-C_7H_{16} to CO_2 and H_2O, 11 moles of molecular oxygen (O_2) are needed, as can be seen in the reaction equation (1) and the graphic illustration in Figure 4, whose graphical representations of the molecular structures were taken from PubChem [28].

$$n\text{-}C_7H_{16} + 11\ O_2 \rightarrow 7\ CO_2 + 8\ H_2O, \tag{1}$$

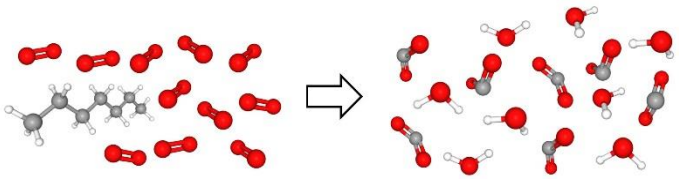

Figure 4. Educts and products during the oxidation of *n*-heptane to carbon dioxide and water. [28]

Although the reaction equation (1) correctly reflects the ratio of educts and products during the oxidation of *n*-C_7H_{16}, a detailed analysis of the combustion process shows that, in addition to the four species *n*-C_7H_{16}, O_2, CO_2 and H_2O, a large number of other species such as smaller alkanes, aldehydes, radicals and many more are also involved in the combustion process. The addition of these other species cannot be explained by the reaction equation (1) and therefore indicates that this equation does not reflect the real course of the reaction. In fact, several reactions occur, inducing the formation of the final products H_2O and CO_2.

As previously mentioned, hydrocarbons remain largely stable under ambient conditions and while in contact with oxygen. To start the reaction, an external energy supply is necessary, like an external heat source. The associated rise in temperature follows the increased molecular movement of the molecules involved. The stronger this movement is, the more likely internal molecular bonds are broken and result in the formation of smaller fragments and radicals. Another possibility of energy coupling is the irradiation with intensive electromagnetic radiation. Radicals are atoms or molecules that have at least one unpaired valence electron like atomic hydrogen (H), atomic oxygen (O) and the hydroxyl radical (OH), which play an important role in the combustion chemistry. Because of this unpaired valence electron, radicals usually show a high reactivity.

Through a closer examination of the chain of reactions that occur during combustion, four different types of chain reactions can be distinguished. If the reaction of two non-radical species induces the formation of at least one radical, this reaction is called chain-initiating. A chain propagation occurs when a radical is consumed by the reaction and a new radical is generated as a product. If the reaction generates more radicals than it consumes, this is referred to as chain branching. A chain termination occurs when a reaction consumes radicals but does not generate new ones. [29]

The oxidation process of hydrocarbons, schematically shown in Figure 5, can be divided into the following basic process steps. The process starts with the formation of hydroperoxides (ROOH), which are generated through events like reacting with the oxygen in the combustion air. Hydroperoxides consist of an organyl group (R) and a functional OOH group. In the next step, the dehydrogenation, a decomposition into smaller hydrocarbons, and the formation of radicals occurs, steps that are essential for the reaction chain to progress. The reactions of the radicals with the smaller hydrocarbons trigger the formation of small alkenes and alkadienes, followed by the formation of aldehydes and then the formation of carbon monoxide (CO), H_2O and molecular hydrogen (H_2). The reaction steps described thus far contribute approximately 40 % to the total heat release. Therefore, most of the heat is released in the last step of the process, when CO and H_2 react to CO_2 and H_2O. [13]

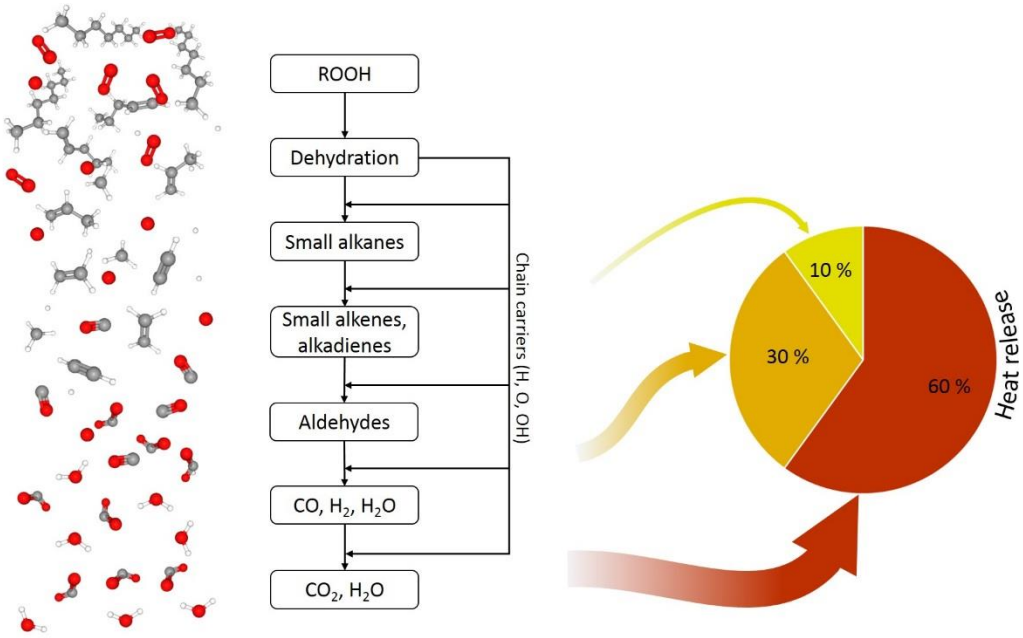

Figure 5. Oxidation scheme of hydrocarbons. [13,28]

3.3 *Auto Ignition Limits*

If the conditions for chain initiation, chain propagation and chain branching occur in a hydrocarbon-air mixture, and chain-branching reactions dominate the reactions leading to chain termination, ignition and combustion of the fuel-air mixture occurs. In case of self-ignition, i.e., without the presence of an external ignition source, the onset of ignition depends on various parameters such as pressure, temperature, mixing ratio and boundary conditions in the reactor. The left side of Figure 6 shows the schematic diagram of ignition limits as a function of pressure and temperature of a stoichiometric hydrogen-oxygen mixture, while the right side demonstrates the more complex diagram for hydrocarbons.

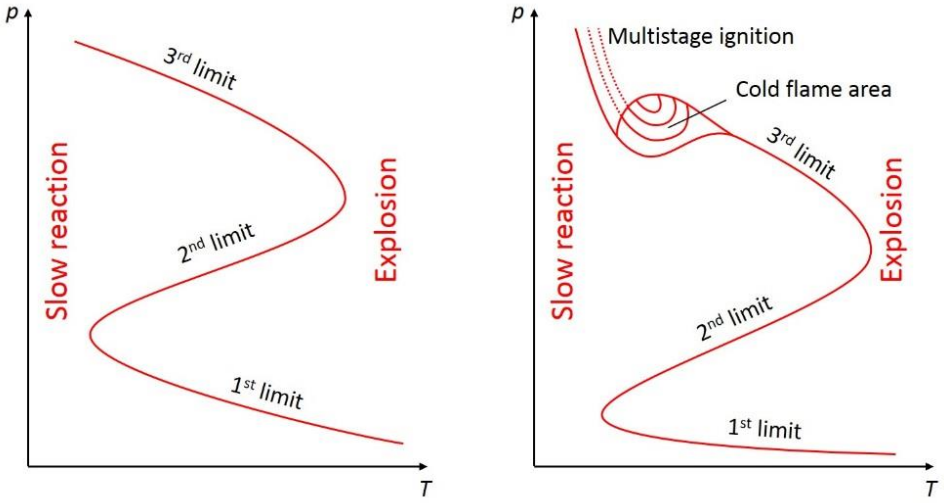

Figure 6. Schematic p-T-explosion diagram for hydrogen (left) and hydrocarbons (right). [29]

Ignition limits differ due to the temperature and pressure dependent transport properties in the gas, as well as the disparate favoring of the sequence of chain branching and chain termination reactions depending on the ambient conditions. The first ignition limit in the hydrogen-oxygen mixture results from too low pressure, which increases the probability that radicals will diffuse to the reactor wall and deactivate there. Only when the pressure is increased and the diffusion rate

decreased do the conditions for successful chain propagation and chain branching occur and trigger spontaneous ignition. The second ignition limit results from the competitive situation between chain branching and chain terminating reactions. By shifting the balance of forces, reactions that lead to chain termination become dominant and the mixture no longer ignites. Competition between heat production by chemical reactions and heat loss through the reactor wall results in the third limit. If this limit is exceeded, the mixture heats up continuously until thermal ignition occurs. [29]

In contrast to the oxidation of hydrogen, an area with cold flames is evident in the case of hydrocarbons as shown on the right side of Figure 6. Using the oxidation of the hydrocarbon methane (CH_4) as an example, this behavior is explained by the interaction of the following three reactions (2), (3) and (4).

$$CH_3 + O_2 \rightleftarrows CH_3O_2, \tag{2}$$

$$CH_3O_2 + CH_4 \rightarrow CH_3OOH + CH_3, \tag{3}$$

$$CH_3OOH \rightarrow CH_3O + OH, \tag{4}$$

If the equilibrium position of reaction (2) is on the right side, equations (2), (3) and (4) represent a chain branching, since more radicals are produced than consumed. With increasing temperature, however, the equilibrium position in reaction (2) shifts to the left, which directly affects the course of reaction (3) and (4) and finally leads to chain termination. [13]

3.4 Ignition Delay Time

Through the examination of a mixture of hydrocarbons and air under ignition conditions, ignition can be determined to occur only after a certain time period, the so-called ignition delay time (IDT), rather than immediately. For descriptive purposes, a stoichiometric methane-air mixture at 920 K and 60 bar is considered. Under these conditions, the mixture ignites, but as shown by the pressure and temperature curve in Figure 7, the mixture ignites after 17.7 ms (indicated by a sharp rise in pressure and temperature) rather than immediately. This behavior is characteristic of radical chain explosions. During the IDT, reactions occur that induce chain branching and thus increase radical concentration, required for the continuation of the ignition process. Because only a relatively small amount of heat is released during these processes, as illustrated by the pie chart in Figure 5, no major change in the temperature can be determined. Finally, the oxidation of CO to CO_2 and H_2 to H_2O releases the most heat, leading to a significant increase in temperature. [29]

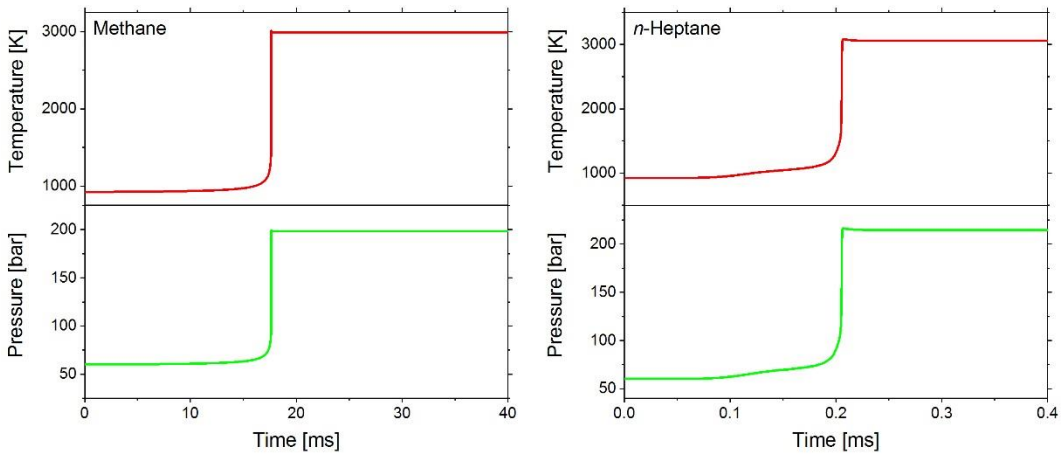

Figure 7. Simulated temperature and pressure curve during ignition of a stoichiometric methane-air mixture (left) and a stoichiometric *n*-heptane-air mixture (right) at 920 K and 60 bar.

A similar course of pressure and temperature can be seen in the ignition process of an *n*-heptane-air mixture, as the right side of Figure 7 shows. A detailed examination reveals an initial temperature rise at 0.1 ms, before the mixture actually ignites at approximately 0.2 ms after the start. This phenomenon, which dominates more as the size of the hydrocarbons increases, is known as two-stage ignition and results from the temperature-dependent shift in the equilibrium position of reaction (5):

$$R + O_2 \leftrightarrow RO_2, \tag{5}$$

$$RO_2 \leftrightarrow ROOH, \tag{6}$$

If the equilibrium position of reaction (5) is on the right side, the subsequent reaction (6) initiates the chain reaction shown in Figure 5. With increasing temperature, the equilibrium position of reaction (5) shifts, leading to an interruption of the chain branching. Instead, reactions become dominant, which lead to the formation of alkenes and hydroperoxyl radicals (HO_2). HO_2 radicals further react to the initially relatively stable hydrogen peroxide (H_2O_2). Only when the temperature reaches a value of about 1000 K after a steady increase in temperature does H_2O_2 decompose into OH radicals and initiate the ignition of the entire mixture. [30]

3.4.1 Temperature Dependency of the Ignition Delay Time

The IDT varies reciprocally and exponentially with the value of the temperature [29]. A graphical representation of the IDT therefore commonly plots the reciprocal of the temperature on the horizontal axis and selects a logarithmic scale for the IDT, shown on the vertical axis. As an example, Figure 8 shows the temperature dependent simulated IDTs of a stoichiometric methane-air, propane-air and *n*-heptane-air mixture at a pressure value of 60 bar using a linear as well as a logarithmic scaling of the vertical axis.

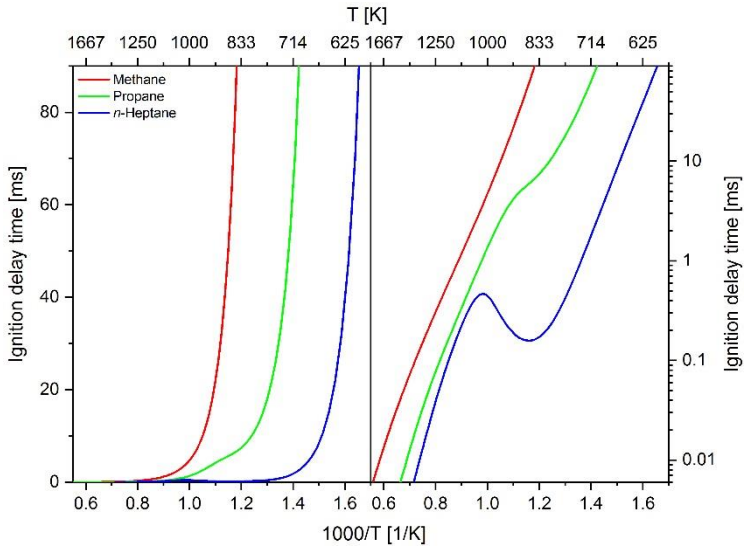

Figure 8. Simulated temperature-dependent ignition delay time of a stoichiometric methane-air, propane-air and *n*-heptane-air mixture at a pressure of 60 bar plotted with a linear (left) and logarithmic (right) scaling of the vertical axis.

The comparison of the two types of presentations shows the advantage of a logarithmic scale. An increase in IDT is evident despite an increasing temperature when examining the *n*-heptane-air mixture in the temperature range 850 to 1000 K. This range is also called a zone with a negative temperature coefficient (NTC). The NTC zone is caused by the occurrence of two-stage ignition, as previously described. A change in the temperature dependency of the IDT in propane mixtures can also be seen in this temperature range. In contrast to *n*-heptane, however, the slope of the IDT as a

function of the reciprocal value of the temperature always remains positive, failing to reveal any NTC zone. Smaller hydrocarbons result in a less pronounced two-stage ignition and the formation of an NTC zone; thus, almost no deviation from the approximate exponential dependence on the reciprocal value of the temperature is apparent in methane.

3.4.2 Experimental Investigation of the Ignition Delay Time

Although the IDT represents a reduction of the complex sequence of the ignition process to a single number, this parameter serves as a relevant characteristic of a fuel-air mixture as a function of equivalence ratio, pressure and temperature and is therefore frequently used in ignition characterization. For example, the IDT represents an important factor in fast-running processes such as the ignition of the fuel-air mixture in a combustion engine. If the mixture ignites too early, knocking occurs and the engine is heavily loaded. If ignition occurs too late, the fuel is no longer burned under optimal conditions; parts of the fuel may therefore remain unburned, increasing pollutant emissions and decreasing the overall efficiency of the engine. In this respect, the ignition behavior and the associated IDT of various fuels as a function of the ambient conditions inspires great interest. Due to this need, different experimental methods have been developed to determine the IDTs of different fuels-air mixtures. For the investigation of homogeneous mixtures, the use of rapid compression machines (RCMs) and shock tubes (STs) has been established. Test facilities like rapid compression expansion machines (RCEMs) and combustion vessels (CVs) can be used to investigate the ignition properties of fuels with inhomogeneous distribution in the combustion chamber (for example due to fuel introduction via injector).

Rapid Compression Machine

When examining the ignitability of a fuel-air mixture with the aid of an RCM, the mixture to be investigated is first composed and afterwards introduced into the combustion chamber as a homogeneous mixture. In order to determine the IDT, the mixture must be abruptly exposed to conditions that cause self-ignition. These conditions are ensured by the RCM piston, which quickly compresses the mixture, before being anchored at the end position. The compression causes a rapid increase in pressure and temperature in the combustion chamber. If this action achieves the conditions for ignition of the mixture, the ignition and combustion occur after the expiry of the IDT. The temperature and pressure values reached after the mixture compression depend on the compression ratio, the temperature and pressure before the start of compression and the exact composition of the mixture. The measured RCM-IDT values used in this thesis were determined with an RCM from the research group PCFC (Physico Chemical Fundamentals of Combustion) at the RWTH Aachen University [31,32]. This system uses a pressure sensor to determine the pressure development in the combustion chamber. By establishing the exact composition of the fuel-air mixture, the temperature curve was derived from the pressure data. A typical curve of the pressure in the combustion chamber is shown in Figure 9. In addition, the individual process steps of the RCM measurement are shown schematically.

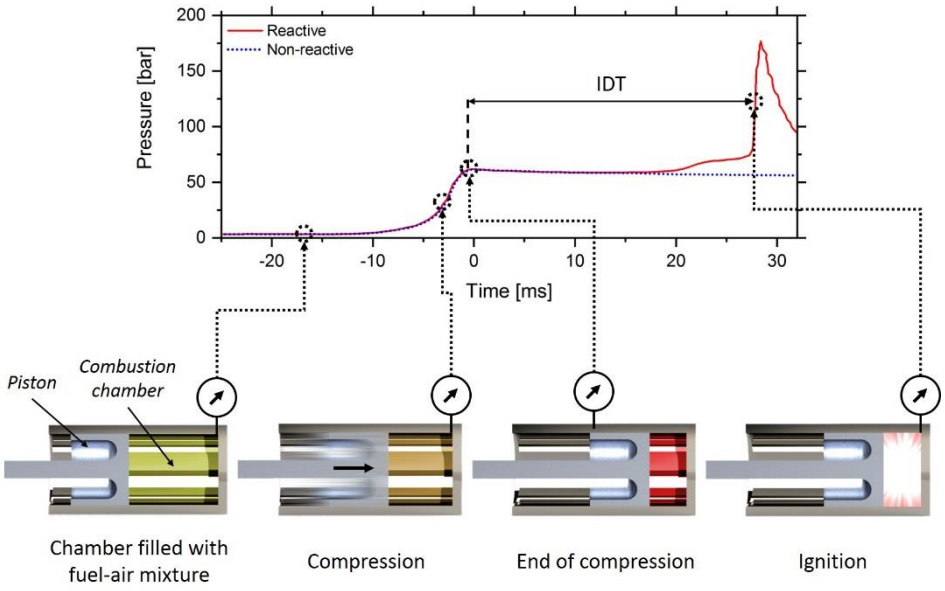

Figure 9. Typical pressure profile of an RCM measurement with successful ignition of the mixture, including a schematic representation of the individual RCM process steps.

The pressure increase from the piston compression does not correspond to a step function but instead shows a certain temporal extension due to the finite speed of the piston. This thesis defined the IDT in the RCM measurements as the time difference between reaching the end position of the piston (end of compression) and the maximum pressure increase due to the ignition of the mixture as indicated in Figure 9. However, this does not represent the only way to define the IDT. For RCMs with optical access, the signal strength of the light emission of excited OH radicals or a tangent line applied to the pressure signal that intersects with a selected horizontal line can also be used to define the IDT. Knowing the exact definition of the IDT is therefore integral to avoid misinterpreting the measured data. Furthermore, the so-called facility effects must be considered when interpreting RCM measurement data. These effects occur, i.a., from the previous formation of radicals in the compression phase; the reaction has thus already begun before the piston reaches its end position. Assuming an undisturbed mixture composition at the end of compression would therefore inevitably result in incorrect findings when comparing these measurements with simulations that did not consider this radical formation. Due to the cold walls of the reaction chamber compared to the compressed hot mixture, the mixture cools down near the wall, thus decreasing the pressure in the combustion chamber. This cooling down is generally coupled with a reduction in the reaction speed and thus an increase in the IDT. To consider the effects in the compression phase as well as the phase between the compression ending and the beginning of ignition in theoretical considerations, a second non-reactive measurement is executed for each RCM measurement by exchanging the oxygen with an inert gas. The resulting pressure curve, indicated as blue dotted line in Figure 9, is used as an input parameter for the simulation. The minimum measurable IDT with an RCM is limited by the time required to compress the mixture. In the case of very short IDTs, ignition may have already occurred in the compression phase, thus preventing evaluation. In this case, a test system that allows even faster compression of the mixture is required, which is possible in an ST.

Shock Tube

In an ST, a shock wave instead of a piston (in contrast to the RCM) compresses the fuel-air mixture under investigation. The ST is divided into a high-pressure and a low-pressure section. The latter section is filled with the fuel-air mixture to be investigated. In the ST of the research group PCFC, which was utilized to determine the IDTs used in this thesis, the two sections are separated from each other by an arrangement of two diaphragms. The pressure between the diaphragms is selected in the test preparation to allow them to withstand the respective pressure differences

between the adjacent sections. The ST measurement is started by abruptly reducing the pressure between the diaphragms, causing them to rupture. A shock wave is generated and propagates through the low-pressure area. After the reflection at the end of the ST, the shock wave propagates in the opposite direction and, due to the pressure superposition, leaves this area with increased pressure and temperature. If pressure and temperature are sufficient for self-ignition to occur, the mixture is ignited after exceeding the IDT. A typical pressure curve for an ST measurement with successful ignition is shown in Figure 10.

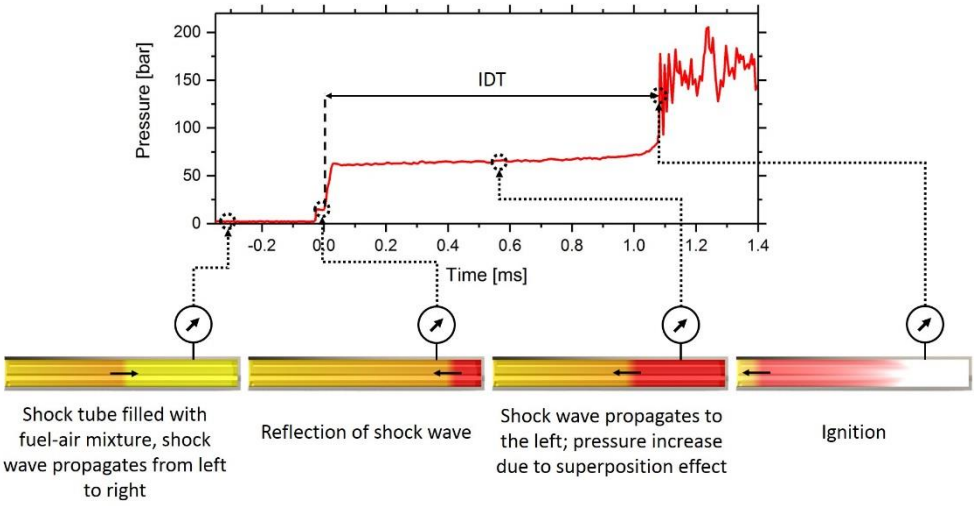

Figure 10. Typical course of an ST pressure profile with successful ignition of the mixture, including a schematic representation of the individual ST process steps.

As can be seen from the pressure curve, the pressure in the ST remains relatively constant after passage of the reflected shock wave, apart from a system-specific slight pressure increase. This pressure increase results from boundary layers and a non-ideal opening of the diaphragms [33,34] and is on average about 8 %/ms in the ST used [31].

Rapid Compression Expansion Machine

In a rapid compression expansion machine (RCEM), the piston is not fixed at maximum compression (in contrast to the RCM), but can move in the opposite direction after compression. The compression ratio obtained depends on the piston position in which a balance is achieved between the force generated by the driving pressure and the counterforce generated by the increase in pressure in the combustion chamber. This setup results in a piston kinematic that is comparable to a normal crank drive around top dead center (TDC) [35]. The measurement results used in this thesis were derived from an RCEM from FAU [35,36]. Measurements were performed by using inhomogeneous mixtures of natural gas, diesel and air. For this purpose, the RCEM combustion chamber was first filled with air or a mixture of natural gas and air. The mixture was compressed by the pneumatically operated piston and a diesel pilot was injected shortly before reaching the TDC. A characteristic pressure curve for an RCEM measurement with successful ignition is shown in Figure 11. To enable a statistical evaluation, the test is performed several times under constant conditions. The deviations of the individual pressure curves are shown in Figure 11 as a red marked fluctuation range.

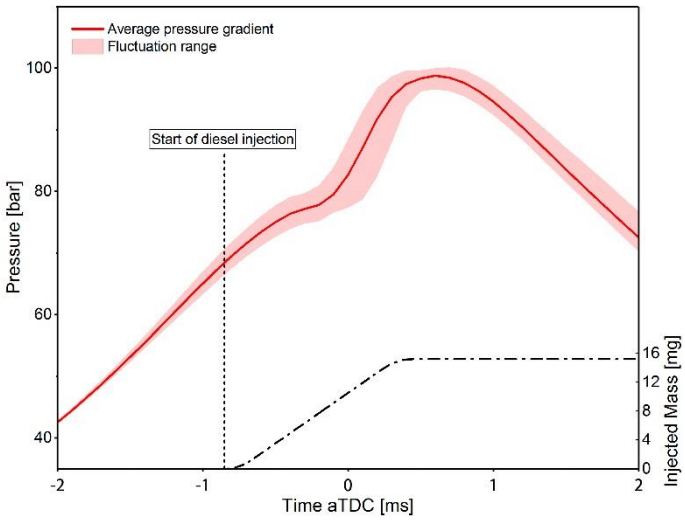

Figure 11. Typical course of an RCEM pressure profile with successful ignition of the mixture. [35]

Combustion Vessel

A combustion vessel was used for the detailed investigation of diesel spray propagation and ignition. The data sets used in this thesis originate from measurements with the CV from FAU [27,36]. To be able to determine the development of the spray and the location of ignition, Mie-scattering was used to identify the liquid phase in the spray plume. To measure the vapor phase, Schlieren-imaging was applied. To detect the area of ignition and analyze the spread of the flame, the electromagnetic radiation was identified in the visible range as well as in the ultraviolet (UV) radiation emitted by OH radicals due to the transition from an excited state to a lower energy level. [35]

Figure 12 demonstrates examples of graphical evaluations of Mie-scattering measurements, Schlieren images and optical recordings in the visible range and the UV emission of OH radicals.

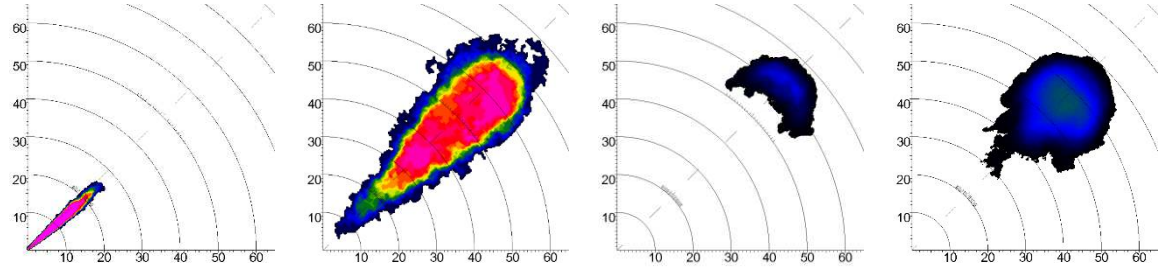

Figure 12. Examples for graphical evaluations of Mie-scattering measurements (first from left), Schlieren images (second from left) as well as optical recordings in the visible range (third from left) and the UV emission of OH radicals (right). [27,35]

3.5 Reaction Mechanism

Detailed knowledge of the exact reaction sequence is necessary to reproduce the ignition process and the subsequent combustion by means of simulations. Such detail requires the knowledge of all important reactions and species involved in the process. Furthermore, information is required on the speed of the respective reactions, the influence of the ambient conditions on the reaction speed, the transport properties necessary to be considered for the individual species or the amount of heat released in the respective reactions. All this information must be defined in the data set contained in the reaction mechanism.

A reaction mechanism usually comprises three parts. The first part contains the gas-phase chemical reactions. The second part includes information about the thermodynamic properties of the involved species and the third part specifies the transport properties of the species.

3.5.1 Reactions

A reaction equation has the general form (7):

$$\nu_a\, A + \nu_B\, B + \nu_C\, C + \cdots \;\underset{k^{(r)}}{\overset{k^{(f)}}{\rightleftarrows}}\; \nu_D\, D + \nu_E\, E + \nu_F\, F + \cdots, \tag{7}$$

$A, B, C, \ldots$ represent the different species involved in the reaction, $\nu_a, \nu_b, \nu_c, \ldots$ are the respective stoichiometric coefficients, and $k^{(f)}$ and $k^{(r)}$ are the speed coefficients of the forward and reverse reaction. When the reaction proceeds in a forward direction, the change in concentration of species A over time can be represented with equation (8):

$$\frac{d[A]}{dt} = -k^{(f)}\,[A]^a\,[B]^b\,[C]^c \ldots, \tag{8}$$

where $a, b, c, \ldots$ are the reaction orders with respect to the species $A, B, C, \ldots$. Assuming that the concentration of species $B, C, \ldots$ change only imperceptibly, perhaps because they are present in abundance, $k^{(f)}\,[B]^b\,[C]^c \ldots$ can be combined to the new reaction rate coefficient k, leading to equation (9):

$$\frac{d[A]}{dt} = -k\,[A]^a, \tag{9}$$

Depending on the reaction order, a specific time-dependent concentration course results. Plots for the first, second and third order reactions are shown schematically in Figure 13 with the reaction rate coefficients $k_1 > k_2 > k_3$. [13]

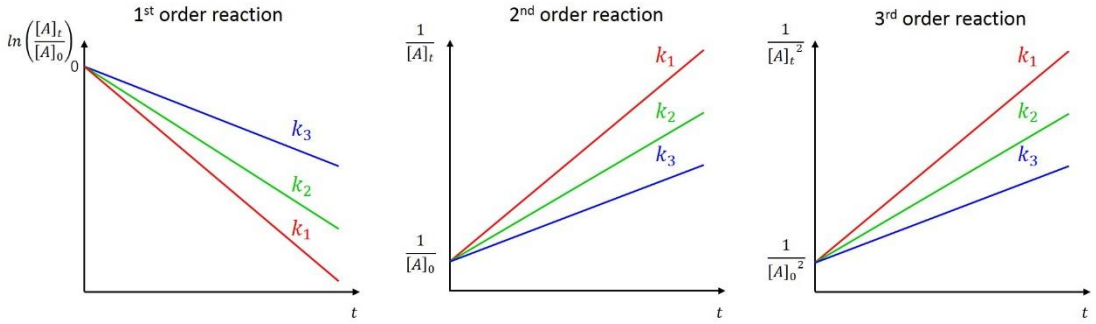

Figure 13. Decay profiles for first, second and third order reactions.

The higher the reaction rate coefficient, the faster the reaction proceeds and the faster the corresponding species concentration decreases. The reaction rate coefficient k_k of species k shows a strong, non-linear temperature dependency, which can be described by the extended Arrhenius approach (10):

$$k_k = A_k\, T^{\beta_k}\, e^{-\frac{E_{A,k}}{R\,T}}, \tag{10}$$

with the pre-exponential factor A_k, the temperature exponent β_k, the activation energy $E_{A,k}$, the temperature T and the universal gas constant R. The activation energy represents the energy required to break bonds to allow the reaction to proceed. The simultaneous formation of new bonds allows a corresponding decrease in the activation energy. The pre-exponential factor possesses a different meaning depending on the type of reaction. In uni-molecular reactions, i.e., only one reactant molecule participates in the reaction, the reciprocal value of the pre-exponential factor corresponds to the average lifetime of the reactant. In the case of a reaction between two reactants (bimolecular reaction), the pre-exponential factor corresponds to the collision factor, which indicates the number of collisions between the reacting molecules per time unit. [29]

Reactions are divided into net and elementary reactions. In the case of elementary reactions, the reaction proceeds exactly as indicated by the reaction equation, i.e., the reaction order corresponds to the reaction molecularity. In this case, the reaction orders given in equation (8) correspond to the stoichiometric coefficients in equation (7). For net reactions, the situation is much more complex, so that the reaction order can be non-integer and even negative. [29]

As an example, the reaction of hydrogen and oxygen to water is examined in more detail. Although the reaction equation (11)

$$2\,H_2 + O_2 \rightarrow 2\,H_2O, \tag{11}$$

correctly characterizes the required quantities of the educts and products, it cannot describe the occurrence of O or OH radicals, for example, which are detectable in measurements. It therefore represents a net rather than elementary reaction. In fact, a total of 37 elementary reactions occur in the reaction of hydrogen and oxygen to water [13]. Three of these elementary reactions, which were copied from a reaction mechanism in Chemkin format, are specified in Figure 14.

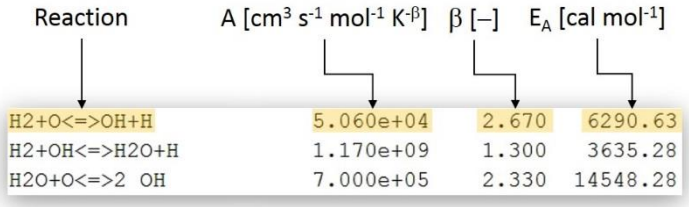

Figure 14. Example of elementary reactions and the corresponding Arrhenius parameters definition extracted from a mechanism in Chemkin format.

For each reaction in the reaction mechanism, the corresponding Arrhenius parameters are defined for the calculation of the temperature-dependent reaction rate coefficients using equation (10).

3.5.2 Thermodynamic Data

To calculate the thermodynamic behavior of the fuel-air mixture in the simulation of the combustion process, thermodynamic information corresponding to each species involved must be included. The standard state molar heat capacity at constant pressure as well as the standard state molar enthalpy and standard state molar entropy are provided for the simulation. With the help of these data, further quantities such as heat capacity at constant volume, internal energy, Gibbs free energy and Helmholtz free energy can be calculated [37]. As an example, Figure 15 shows an excerpt of the thermodynamic definition of the OH radical. It includes the definition of the species, the number of elements contained in the species, the state of aggregation, temperature values for the definition of the upper and lower temperature interval and 14 numerical values. These values are required for the calculation of thermodynamic properties using the NASA chemical equilibrium code [37] (equation (12) to (14)). To calculate the thermodynamic properties in the lower temperature interval, the coefficients a_1 to a_7 in the polynomials (12) to (14) correspond to the first seven numbers in the thermodynamics file, which are highlighted in green in Figure 15. The coefficients marked in red are used to calculate the thermodynamic properties in the upper temperature interval.

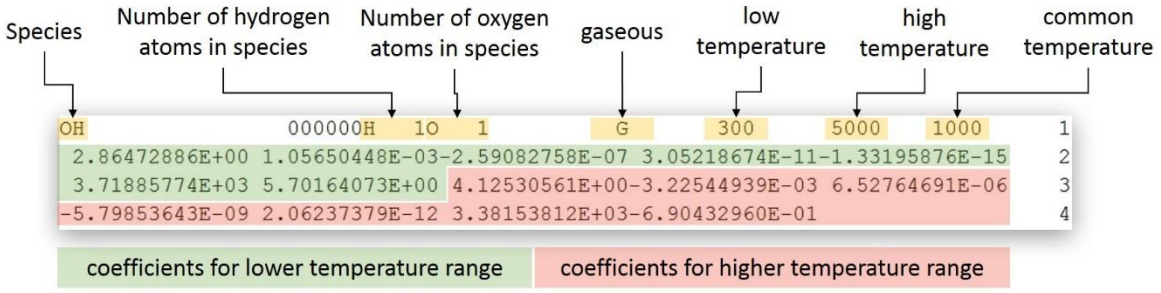

Figure 15. Mechanism extract of the thermodynamics definition of the OH radical.

$$\frac{C_{pk}^0}{R} = a_{1k} + a_{2k}\,T_k + a_{3k}\,{T_k}^2 + a_{4k}\,{T_k}^3 + a_{5k}\,{T_k}^4, \tag{12}$$

$$\frac{H_k^0}{R\,T_k} = a_{1k} + \frac{a_{2k}}{2}T_k + \frac{a_{3k}}{3}\,{T_k}^2 + \frac{a_{4k}}{4}\,{T_k}^3 + \frac{a_{5k}}{5}\,{T_k}^4 + \frac{a_{6k}}{T_k}, \tag{13}$$

$$\frac{S_k^o}{R} = a_{1k}\,ln(T_k) + a_{2k}\,T_k + \frac{a_{3k}}{2}\,{T_k}^2 + \frac{a_{4k}}{3}\,{T_k}^3 + \frac{a_{5k}}{4}\,{T_k}^4 + a_{7k}, \tag{14}$$

3.5.3 Transport Data

In the mixture of atoms and molecules in the combustion chamber, interactions between the species result in the transport of various physical quantities. In a simplified model of interactions at the atomic level, the concept of temperature represents the disordered movement of atoms and molecules, which gains strength as temperature increases. Binding forces between the particles cause the transfer and subsequent propagation of this movement to areas with a lower level of movement, i.e., lower temperature. The speed of the process of transferring energy in the form of heat is measured by thermal conductivity. In the case of an ordered movement in a preferred direction in the gas, i.e., a gas flow, the interaction of atoms and molecules results in the transfer of momentum to regions of the gas with a relatively lower velocity. The strength of this momentum transfer is measured by the gas's viscosity. Due to the tendency of a closed system to assume the state of maximum entropy, differences in concentration within the gas cause mass shifts to achieve an even distribution of all species in the available space. This process is quantified by the gas's level of diffusion.

Thus, to properly assess the transport processes occurring in the gas, its thermal conductivity, viscosity and diffusivity must be known. Accordingly, the transport data file includes all data necessary to calculate the three mentioned properties of each species contained in the mixture. These data consist of the Lennard-Jones potential well depth, Lennard-Jones collision diameter, dipole moment, polarizability, and the rotational relaxation collision number at 298 K [37]. Figure 16 shows a mechanism excerpt of the transport parameters for calculating the transport processes for the OH radical.

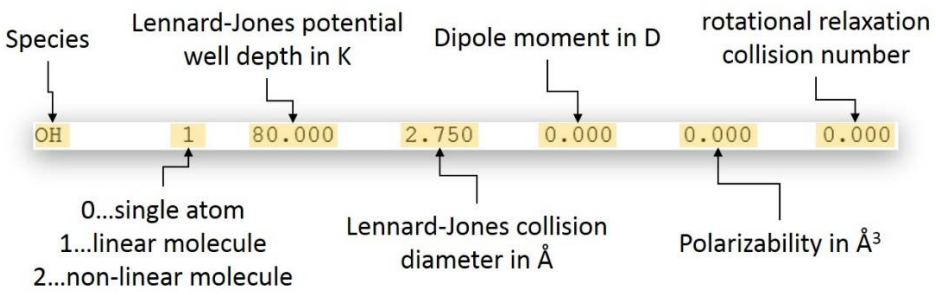

Figure 16. Mechanism extract of the transport characteristic definition of the OH radical.

3.5.4 Mechanism Size

As previously mentioned, 37 elementary reactions are needed to describe the combustion of the simply structured species H_2 and O_2 to H_2O. An increase in the complexity of the species involved and/or the number of educts involved in the combustion process expands the number of elementary reactions required to correctly reproduce the combustion process. Reaction mechanisms for hydrocarbons thus partly consist of several thousand elementary reactions [29].

However, an increase in the number of elementary reactions and thus the size of the mechanism requires a simulation of the combustion process that is more computational and time-intensive. The size of the mechanism used for the calculation of the reaction sequences therefore represents a critical parameter, especially for the time- and space-resolved computationally intensive CFD simulation. Of all elementary reactions, only a few determine the speed of the reaction process. Furthermore, when considering which and to what extent reactions are involved in the combustion process, the removal of several reactions from the reaction mechanism causes a barely visible influence on the simulation result. However, this statement cannot be generalized but depends on the parameter range under consideration. A common method to reduce the computational effort involves decreasing the size of the reaction mechanism by removing reactions that play a subordinate role in the description of the combustion process or combining several successive reactions into one lumped reaction. The progressive reduction in the size of the reaction mechanism results in an increasing deterioration in the reproduction of the combustion process or a restriction in the parameter range in which the reaction mechanism can be used.

3.6 Analysis of Reaction Mechanisms

Reaction mechanisms consist of several hundred to thousands of reactions. To adapt the characteristics of a mechanism, researchers must understand which reactions decisively drive the behavior of the mechanism. In this thesis, two analysis methods were used to investigate reaction mechanisms in detail. With the help of sensitivity analyses, rate-determining reactions were identified. In order to determine characteristic reaction paths, flow analyses were performed.

3.6.1 Sensitivity Analysis

The sensitivity analysis provides insight into the influence of reactions and species on the overall behavior of the reaction mechanism. A larger absolute value of sensitivity indicates a stronger influence of a reaction or species on the reaction process. The time-dependent change of the concentration c of species i of a mechanism consisting of R reactions and considering S species can generally be represented by Equation (15) [29,38]:

$$\frac{dc_i}{dt} = F_i(c_1, \dots, c_S; \kappa_1, \dots, \kappa_R), \tag{15}$$

where κ represents the parameters of the system. All equations defined by (15) for the S species form a system of ordinary differential equations. The solution of the system depends on both the initial conditions, i.e., the starting concentrations, and the parameters κ of the system. In general, the sensitivity $S_{i,r}$ describes how the solution c_i of the equation system depends on the parameter κ_r and is mathematically written as the partial derivative (16) [29]:

$$S_{i,r} = \frac{\partial c_i}{\partial \kappa_r}, \tag{16}$$

All sensitivity analyses in this thesis were performed with LOGEresearch [39], which also considered species flow [40]. Sensitivity analysis targets in LOGEresearch are all species occurring in the mechanism as well as the temperature. To determine the influence of the reactions of the mechanism on the IDT, the CH radical as well as the temperature were used as analysis targets. As

described in detail in Paper II, the CH radical is significantly concentrated in the gas only shortly before ignition, decreasing by several orders of magnitude afterwards. This result indicated that reactions with a large influence on the concentration change of the CH radicals subsequently strongly influence the ignition process itself. Ji et al. [41] found a strong correlation between the IDT sensitivity and the sensitivity towards temperature. This parameter was used for the sensitivity analysis performed in Paper III.

The sensitivity value shows a time dependency; a strong increase is observed near ignition. Since this thesis's investigations focused mainly on the ignition process, the sensitivity values afterwards were not taken into account. Thus, the analysis considered the course of sensitivity until ignition, searching for the maximum sensitivity value (positive or negative) in this time interval. As an example, Figure 17 shows the sensitivity towards temperature of the reaction n-C_7H_{16} + OH ↔ H_2O + n-C_7H_{15} as well as the pressure curve and the first derivative of the pressure curve, which was simulated with a mixture consisting of methane, propane and n-heptane. Ignition is defined as the point at which the pressure increase is at its maximum; that is, the first derivative of the pressure increase is at its maximum value. The area marked in blue indicates the time interval in which the maximum sensitivity value was searched for.

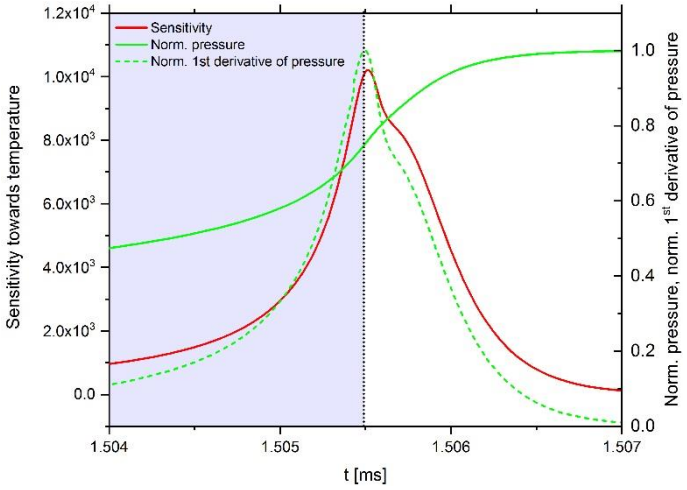

Figure 17. Simulated time-dependent sensitivity towards temperature of the reaction n-C_7H_{16} + OH ↔ H_2O + n-C_7H_{15} as well as the pressure profile in the area of ignition. [42]

This analysis was performed for each reaction considered by the mechanism. Depending on the given problem, the analysis was performed at different temperatures and fuel-air equivalence ratios to analyze the course of sensitivity as a function of temperature and fuel-air equivalence ratio respectively. As an example, Figure 18 shows the temperature-dependent sensitivity curve of the most sensitive reactions when examining a methane-propane-n-heptane mixture.

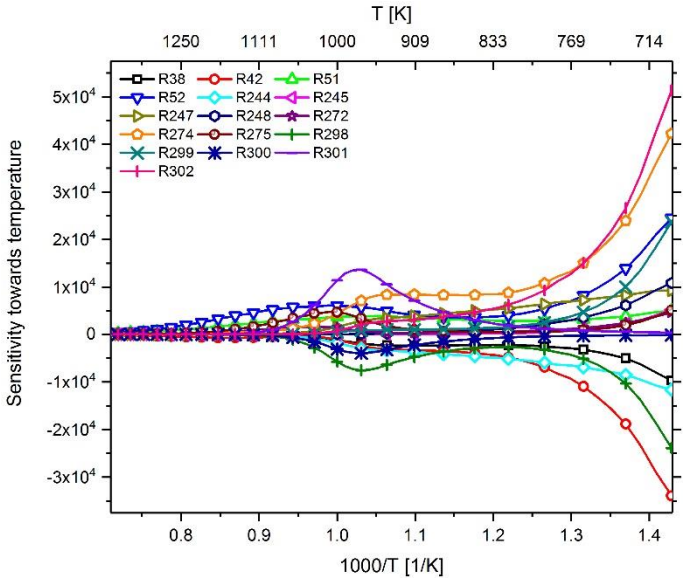

Figure 18. Reaction sensitivity towards temperature simulated with a methane-propane-*n*-heptane mixture. [42]

3.6.2 Flow Analysis

A flow analysis is used to determine which species are consumed and formed by the reactions of the mechanism and to gain insight into the respective consumption and formation rates. With this information, it is possible to map reaction flows, i.e., to determine the typical sequences of species and the reactions involved. In combination with the results of a sensitivity analysis, the influence of a reaction on the overall behavior of the mechanism can thus be better assessed. If a reaction shows a high sensitivity, but plays a subordinate role in the flow analysis, its influence must be evaluated differently than if this reaction is involved in large species flows. An example for the execution of a flow analysis with LOGEresearch is shown in Figure 19, which was performed with a methane-air mixture at 1000 K, 100 bar and a fuel-air equivalence ratio of 0.526. The calculated IDT is 3.532 ms. The flow chart indicates the flows occurred during the time interval of 3.528 to 3.564 ms. In this example, the net flows are given in percent. The pie chart in Figure 19 shows the species that form or react further with CH_3. The bottom right diagram demonstrates the reactions involved in the consumption and formation of CH_4 and CH_3 as well as the species fluxes as a function of time.

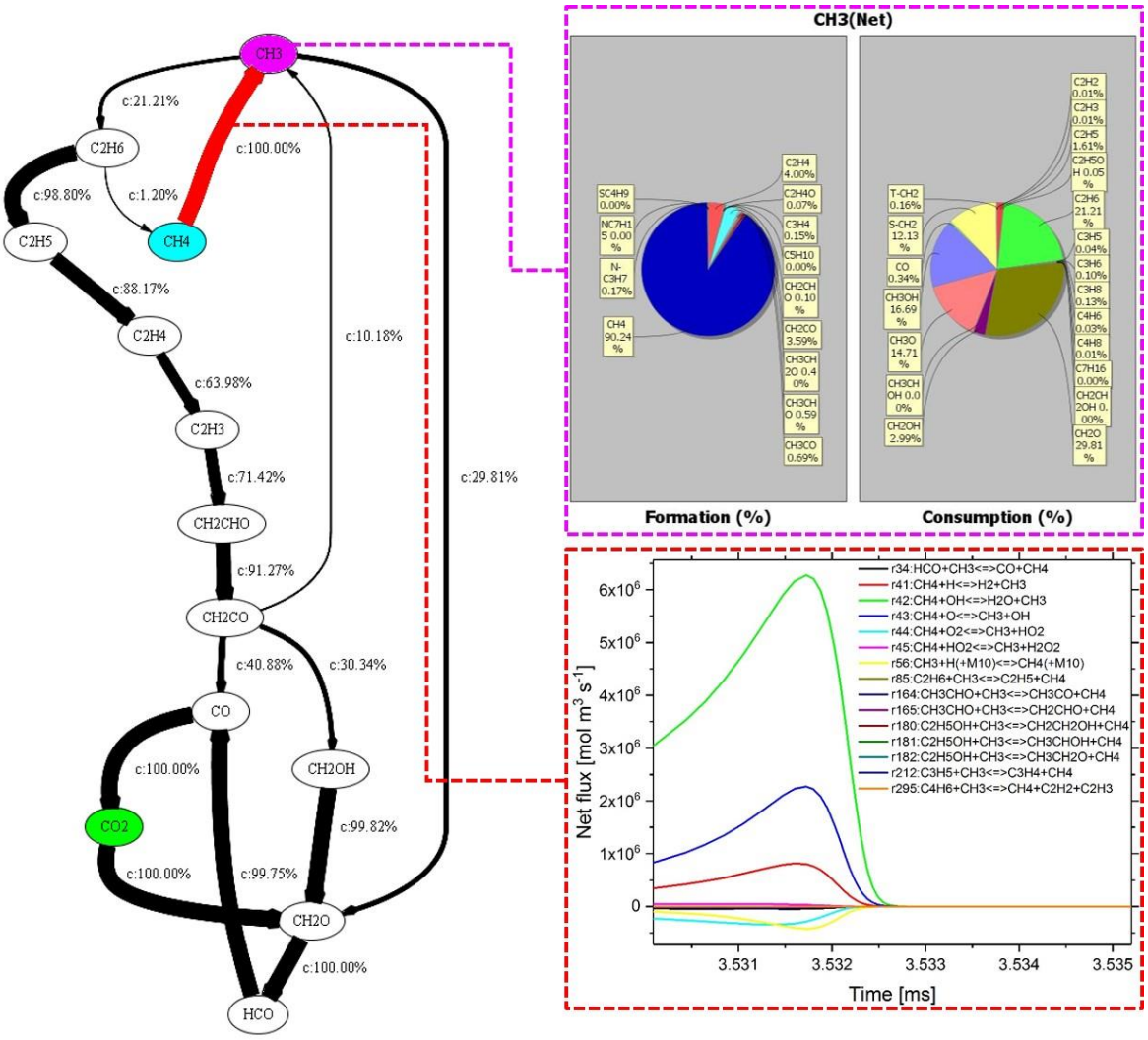

Figure 19. Reaction flow analysis performed with LOGEresearch for combustion of a methane-air mixture in the area of the ignition point. Additionally, those reactions that consume CH_4 and form CH_3 or vice versa are given as examples. The pie charts show the proportion of the species which are consumed or formed during the formation or consumption of the species CH_3.

3.7 Laminar Flame Speed

In the dual fuel engine, as previously explained, ignition is achieved by injecting a diesel pilot into the compressed natural gas-air mixture. Once ignition has occurred, the flame front spreads throughout the entire combustion chamber. Apart from the turbulent flows present in the combustion chamber, the speed of the flame front propagation depends on the laminar flame speed achieved. The oxidation of large aliphatic hydrocarbons is initiated by O, H and OH attacking C-H bonds and forming a radical residual molecule, which further induces formation of alkene and a smaller radical through thermal decay. Regardless of the size of the aliphatic hydrocarbon at the beginning, the oxidation process generally triggers the formation of methyl (CH_3) and ethyl (C_2H_5) radicals. Since they possess a relatively high stability, the oxidation of CH_3 and C_2H_5 is the rate-determining factor, thus justifying the similarity of the combustion of all alkanes and alkenes. The hydrocarbon oxidation is characterized by a hierarchic structure, as can be seen in Figure 20. [29]

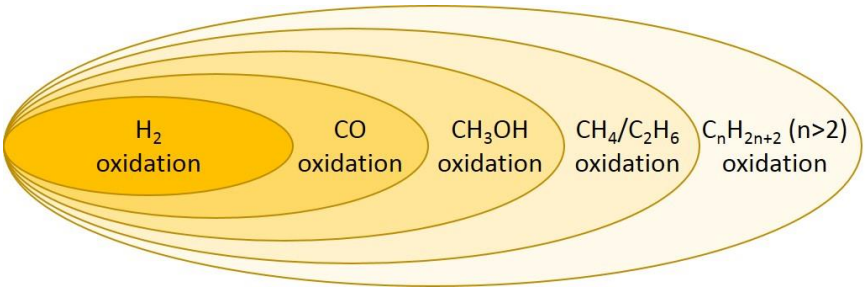

Figure 20. Hierarchical structure of the oxidation of aliphatic hydrocarbons. [29]

Since natural gas and air are already mixed in the dual fuel engine when the combustion chamber is filled, the laminar flame speed of a premixed flame must be considered when examining the flame front propagating into the background gas of the combustion chamber. Essentially, the movement of the flame front is based on chemical, diffusive and convective effects. The flame is composed of three zones: the preheating zone, the reaction zone and the oxidation zone. Reaction rates are slow in the preheating zone due to its low temperatures. These rates accelerate in the adjacent and very thin reaction zone. In the oxidation zone, the final oxidation of CO and H_2 takes place. As shown in Figure 5, the most heat is released in this zone. [43]

Figure 21 shows the spatially resolved mole fraction of the species CH_4, O_2, H_2, CO, CO_2 and H_2O; it also demonstrates the temperature profile and the local flow velocity as a result of a laminar flame speed simulation with LOGEresearch using a methane-air mixture at 10 bar, 400 K and a fuel-air equivalence ratio of 1. The calculated laminar flame speed is 23.17 cm/s, which thus corresponds to the speed with which the unburned gas flows from the left side in Figure 21 to the right towards the flame front. The results of the flame speed simulation with a methane-air mixture and an extended parameter range by the variation of temperature and fuel-air equivalence ratio are shown in a 3D-plot in Figure 22.

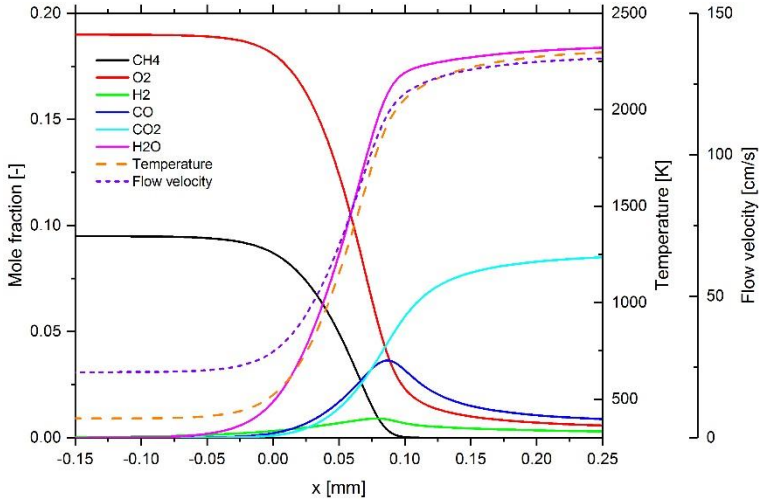

Figure 21. Calculated species, velocity and temperature profile of a flame speed simulation performed with LOGEresearch using a methane-air mixture at 10 bar, 400 K and a fuel-air equivalence ratio of 1.

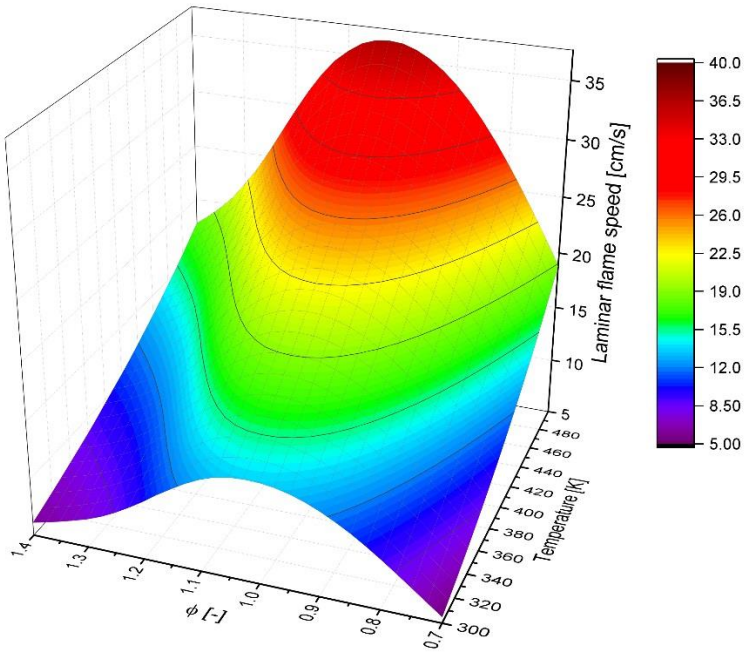

Figure 22. Simulated laminar flame speed of a methane-air mixture at 10 bar as a function of temperature and fuel-air equivalence ratio ϕ using LOGEresearch.

4 Results and Discussions

To evaluate the accuracy of a combustion simulation, experimentally determined values are required for comparison purposes. Within the framework of the investigations of ignition properties, both homogeneous and inhomogeneous mixtures were examined experimentally using an RCM, ST, RCEM and CV and were compared with the results of 0D simulations as well as 3D CFD simulations. 1D simulations were performed and compared with experimental data from the literature when studying laminar flame speeds.

4.1 Investigation of Homogeneus Mixtures

During an investigation of the dual fuel combustion process, the ignition behavior of homogeneous fuel mixtures was measured with the aid of an RCM and ST by the research group PCFC of RWTH Aachen University. As discussed in chapter 3.1, substitute fuels had to be defined to perform simulations with species-rich fuels. In this study, *n*-heptane was used as a diesel substitute and a mixture of methane and propane as a substitute for natural gas. The operating conditions of a 1-cylinder dual fuel test engine [44] were considered when selecting the composition and test conditions of the homogeneous mixtures to be investigated with the RCM and ST. An overview of the experimentally examined mixtures is listed in Table 1. In addition, the experimental data were supplemented with measured IDTs from a previous study [32], in which methane-propane mixtures were investigated with the same test facilities.

Table 1. Overview of the homogeneous mixtures investigated theoretically and experimentally with an RCM and ST, including the respective proportion of methane, propane and *n*-heptane in the mixture, each in mol%, the fuel-air equivalence ratio ϕ, the pressure p in bar, and the temperature T in K. [42]

Test facility	Mix	Fuel composition			ϕ	p	T	Ref.
		CH_4 [mol%]	C_3H_8 [mol%]	C_7H_{16} [mol%]	[–]	[bar]	[K]	
Rapid compression machine	1	100	0	0	0.526	100	906 – 941	[32]
	2	95	5	0	0.526	100	888 – 916	[32]
	3	90	10	0	0.526	100	803 – 898	[31]
	4	70	30	0	0.526	100	826 – 865	[32]
	5	92.68	4.88	2.44	0.594	60	701 – 877	[31]
	6	90.48	4.76	4.76	0.661	60	671 – 781	[31]
	7	92.68	4.88	2.44	0.594	100	709 – 817	[31]
	8	97.56	0	2.44	0.599	60	720 – 869	[31]
Shock tube	9	86.36	4.55	9.09	0.796	60	748 – 1187	[31]
	10	90.91	0	9.09	0.816	60	785 – 1284	[31]

4.1.1 Comparison of Reaction Mechanisms

Based on the definition of *n*-heptane as a diesel substitute, mechanisms available in the literature for the simulation of the IDT were selected and evaluated using the software LOGEresearch. Notably, the available mechanisms differ, in part considerably, in the number of reactions and species included. As part of the investigations published in Paper I, the four *n*-heptane mechanisms of Huang et al. [45], Cai et al. [46], Mehl et al. (Lawrence Livermore National Laboratory (LLNL) *n*-heptane mechanism v3.1) [47] and Zhang et al. [48] were examined in detail. Additionally, the mechanisms AramcoMech 1.3 [49], 2.0 [50] and 3.0 [51] were used for simulation purposes in methane-propane mixtures (mixes 1 to 4 in Table 1). The number of reactions and species considered in each mechanism is compared in Figure 23.

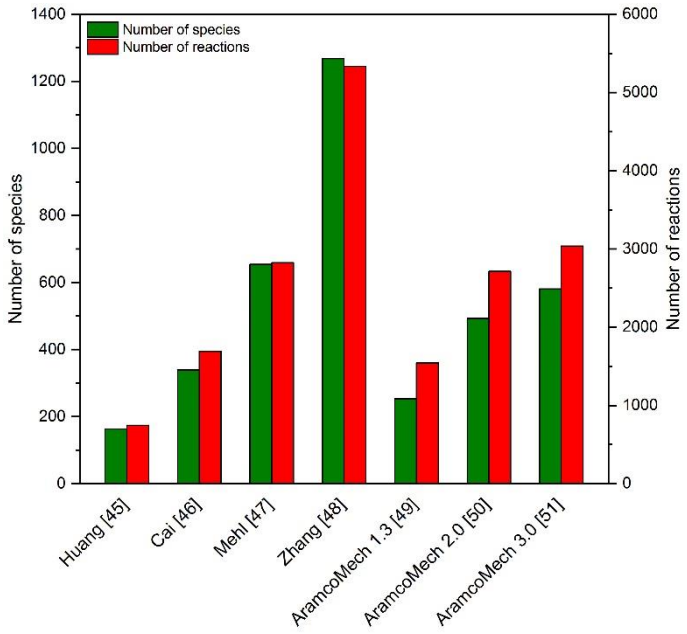

Figure 23. Number of species and reactions of the reaction mechanisms investigated in Paper I.

Due to the choice of the investigated mixture compositions and ambient conditions, Paper I focused its analyses on the following three topics: influence of propane, influence of *n*-heptane and influence of pressure on the IDT.

When considering methane-propane mixtures (mixes 1 to 4 in Table 1), the simulation results with the mechanisms AramcoMech 1.3 and 3.0 showed the smallest deviations from the experimental values. From the *n*-heptane mechanisms investigated, the mechanism of Zhang et al. and the LLNL *n*-heptane mechanism v3.1 could best reproduce the experimental values as shown in Figure 24 and Figure 25.

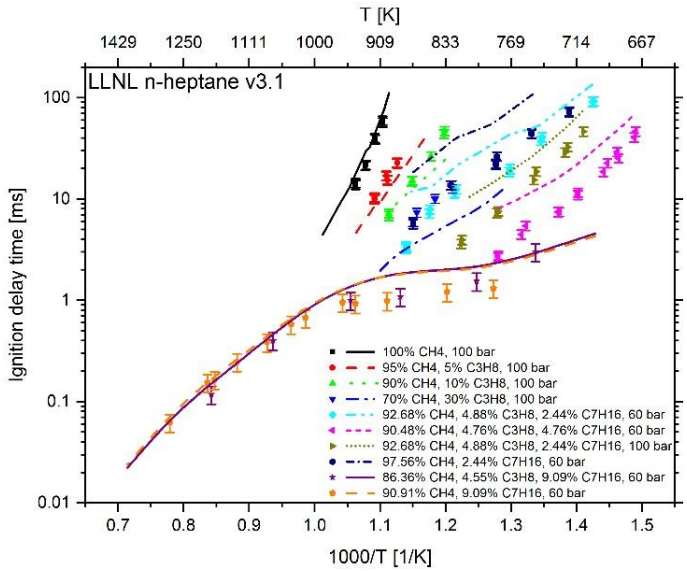

Figure 24. Experimental data (symbols) versus model prediction (lines) using the mechanism LLNL *n*-heptane v3.1. [20]

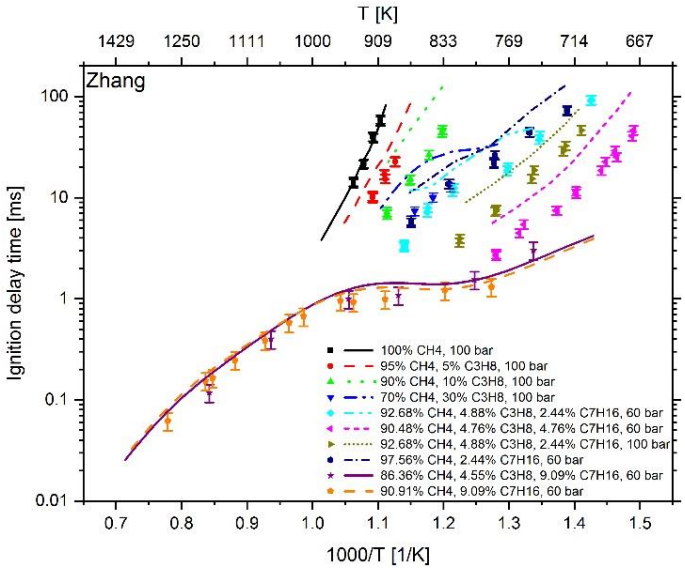

Figure 25. Experimental data (symbols) versus model prediction (lines) using the mechanism of Zhang et al. [20]

However, none of the mechanisms tested were capable of adequately reproducing the measured IDTs under all conditions considered. The search for appropriate mechanisms was therefore extended. Promising results were obtained using the Complete San Diego mechanism with *n*-heptane extension. Figure 26 compares the difference between measured and calculated IDTs in Zhang et. al's mechanisms as well as the LLNL *n*-heptane v3.1 and San Diego mechanism. The exact procedure for calculating the difference is described in Paper II.

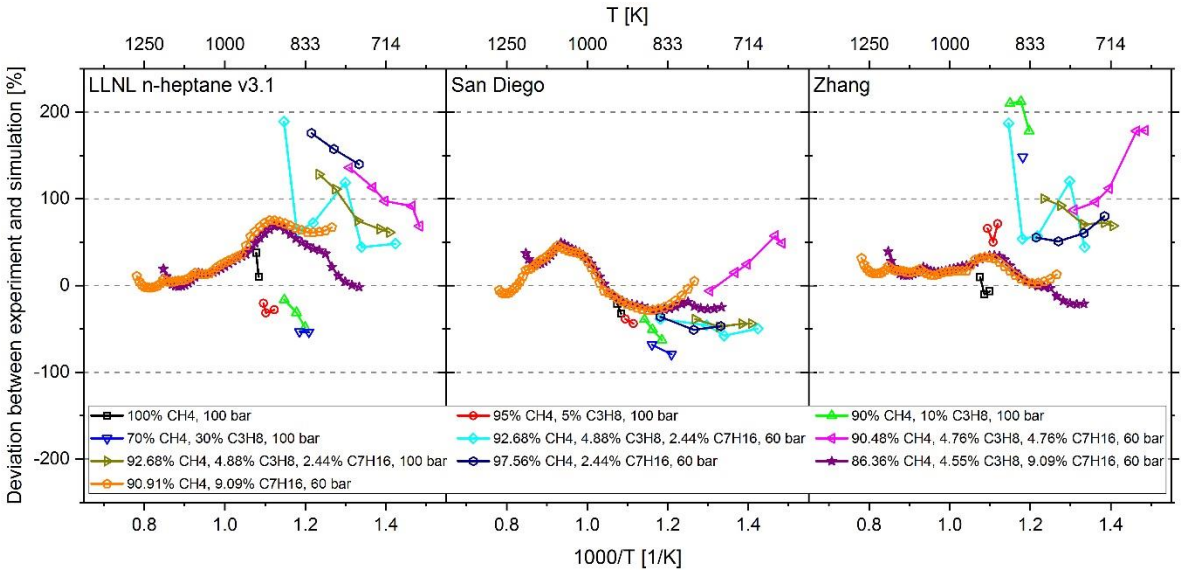

Figure 26. Percentage deviation between measured and calculated IDTs using the mechanism LLNL *n*-heptane v3.1 (left), Complete San Diego mechanism with *n*-heptane extension (middle) and the mechanism of Zhang et al. (right). [20]

The Complete San Diego mechanism with *n*-heptane extension is very compact, comprising about 300 reactions. In comparison, the LLNL *n*-heptane mechanism v3.1 considers almost 3000 reactions, while Zhang's mechanism contains more than 5000 reactions. Due to its success in reproducing the experimental values as well as its compactness, an important characteristic in CFD simulations, the Complete San Diego mechanism with *n*-heptane extension was selected for further investigations.

4.2 *Investigation of Inhomogeneus Mixtures*

The investigation of inhomogeneous mixtures was performed with the help of CFD simulations. The CFD simulations themselves were implemented at the Institute for Powertrains and Automotive Technology of the TU Wien. To validate the simulation results, the RCEM and CV measurement data previously determined at FAU were used [27,35]. The comparison between the CFD simulations and the experimentally determined values as well as the conclusions drawn from this motivated the optimization of the basic mechanism. The optimization process is described in detail in Paper II.

4.2.1 Deviations between Measurements and Simulations

The comparison between simulation and CV-experiment at a chamber pressure of 60 bar, at which diesel was injected into air, showed that at low temperatures (550°C) the simulation underestimated the IDT, whereas an overestimation occurred at higher temperature (700°C) as shown in Figure 27. Figure 28 presents a comparison of the RCEM simulations and experiments, which indicates that the injection of diesel into compressed air resulted in a good reproduction of the IDT under the given conditions, but the injection into a methane-air mixture caused the simulation to strongly overestimate the IDT.

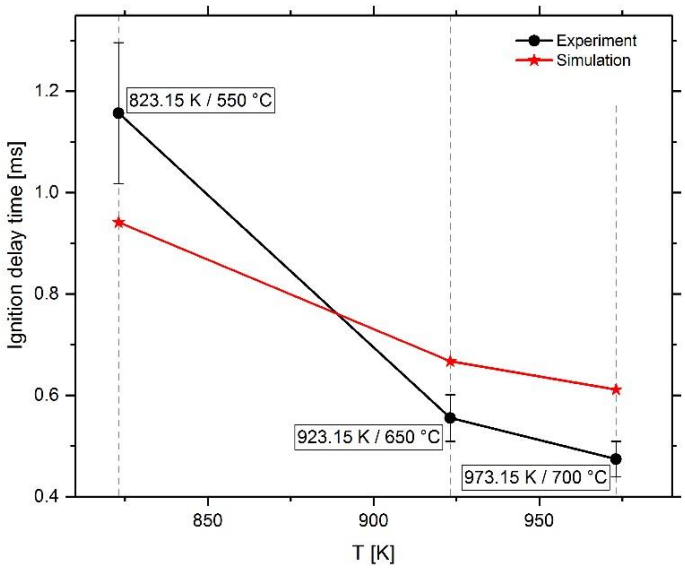

Figure 27. Measured and simulated IDT of pilot fuel in air as a function of temperature. [20]

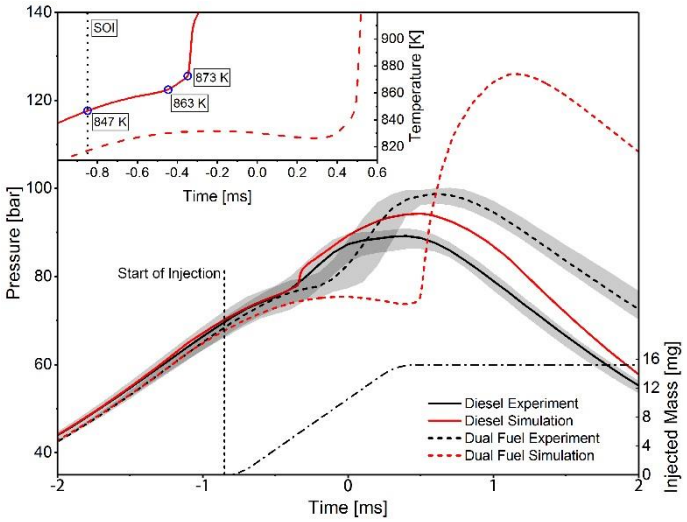

Figure 28. Pressure traces from the CFD simulation and measured values from a RCEM for diesel and dual fuel combustion with 20 % energetic diesel share. The diagram in the top left corner shows the corresponding simulated temperature traces. [20]

4.2.2 Mechanism Analysis

The deviations detected motivated the adaptation of the reaction mechanism, which focused on the adjustment of the *n*-heptane sub-mechanism and the methane chemistry. To determine which reactions in the respective temperature range can strongly influence the IDT, sensitivity analyses were performed on the species CH with an *n*-heptane-air mixture and *n*-heptane-methane-air mixtures with different methane contents. The analyses were performed with LOGEresearch at fuel-lean, stoichiometric and fuel-rich conditions to assess the influence of the fuel-air equivalence ratio on the sensitivity. The results are shown in Figure 29 and Figure 30. Through the additional use of a flow analysis, the most suitable reactions for mechanism optimization were selected. In total, eight reactions have been chosen to optimize the reaction mechanism.

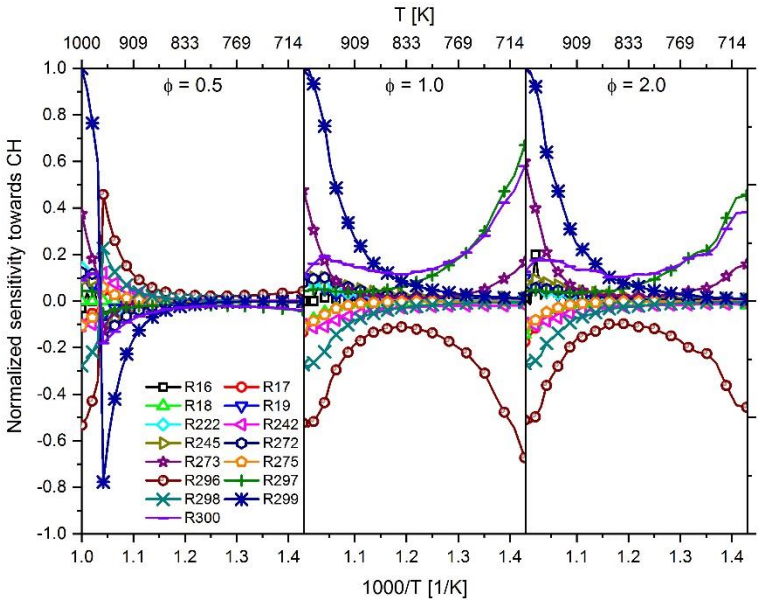

Figure 29. Temperature-dependent sensitivity towards CH of the most sensitive reactions using an *n*-heptane-air mixture at 60 bar and a fuel-air equivalence ratio of 0.5, 1.0 and 2.0 for the simulation process. [20]

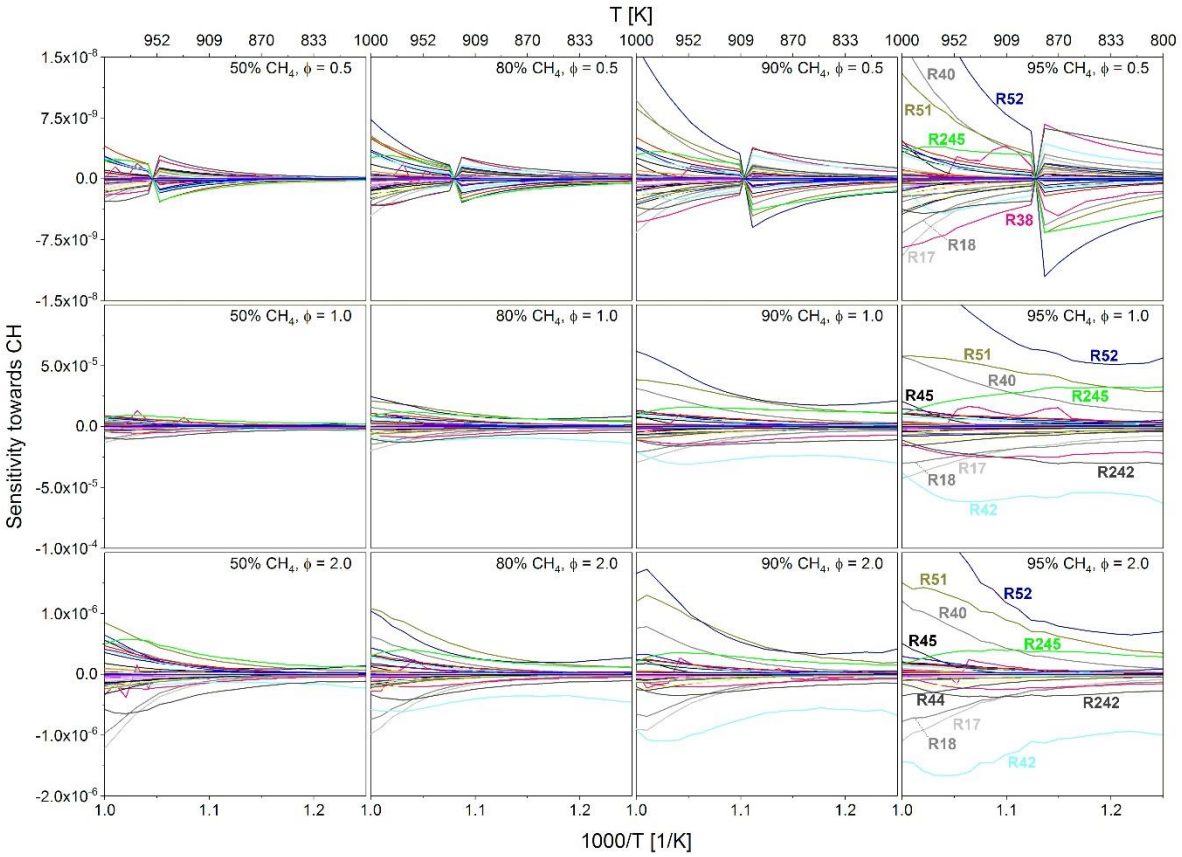

Figure 30. Sensitivity towards CH for methane-*n*-heptane-air mixtures with a methane content between 50 and 95 mol% in the temperature range of 800 to 1000 K, pressure of 60 bar and a fuel-air equivalence ratio of 0.5, 1.0 and 2.0. [20]

4.2.3 Mechanism Adaption

The characteristics of a reaction mechanism can be changed by adjusting the:

- Arrhenius parameters of the corresponding reactions
- Third body collision coefficients
- LOW and TROE parameters [37]
- Transport data
- Thermodynamic data

The optimization process performed in this thesis focused on adapting the Arrhenius parameters, resulting in a change in the reaction rate coefficients of the associated reactions. To assess the extent to which a change in the reaction rate coefficient can be justified by data from the literature, relevant data sets from the National Institute of Standards and Technology (NIST) chemical kinetics database [52], where available, were employed. Using this data as a reference, the reaction rate coefficients were calculated for each data set in the specified temperature interval with a temperature resolution of 1 K. With these data points, a nonlinear fitting based on the extended Arrhenius approach (10) was performed, including the 95 % confidence band and the 95 % prediction band of the fit function. As an example, Figure 31 shows the comparison of the reaction rate coefficient of reaction $CH_4 + OH \leftrightarrow H_2O + CH_3$ before and after the adaption, as well as the fit function and the corresponding confidence and prediction band.

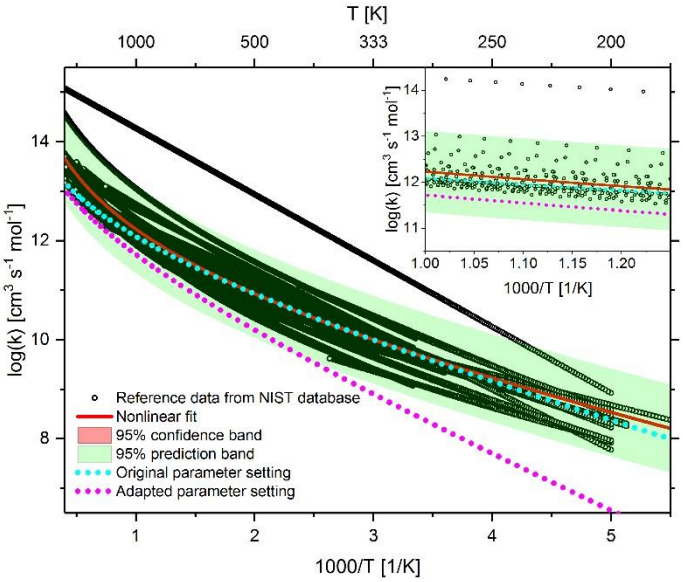

Figure 31. Comparison of the reaction rate coefficient of reaction $CH_4 + OH \leftrightarrow H_2O + CH_3$ before and after adaption as well as the fitted rate coefficient using reference data from the NIST database. [20]

The performed mechanism adjustment in Paper II mainly aimed to minimize the difference between the measured RCEM and CV values and the corresponding CFD simulation results. The parameter changes carried out for this purpose and the resulting changes in the reaction rate constants appeared quite large for some temperature ranges, as can be seen in Figure 31, resulting in a specific field of application for the mechanism. In addition to using the IDT as a reference parameter, the comparison between the measured ignition zone position at the edge of the spray and the spread of the flame with CFD simulation results was also employed to determine the direction of development of the mechanism. The adjustments then made allowed the reduction of the deviations between the experimental values and CFD simulation, at some points significantly, as shown in Figure 32 and Figure 33.

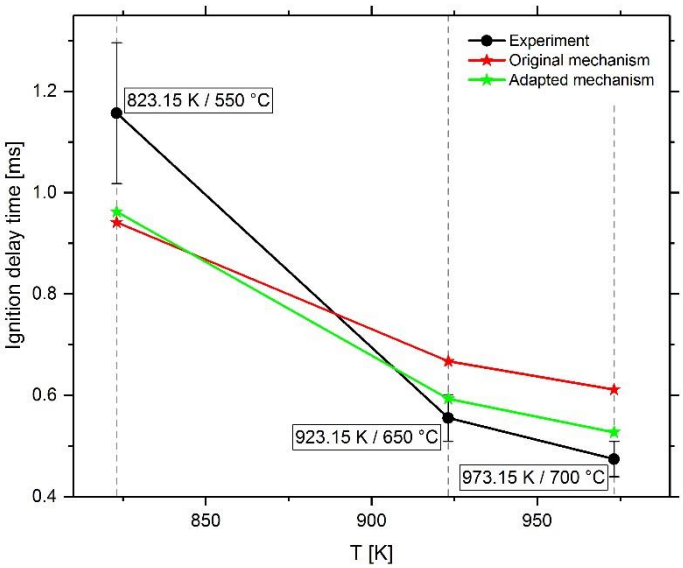

Figure 32. Comparison of measurements and CFD-simulation results using the mechanism before and after the optimization process. [20]

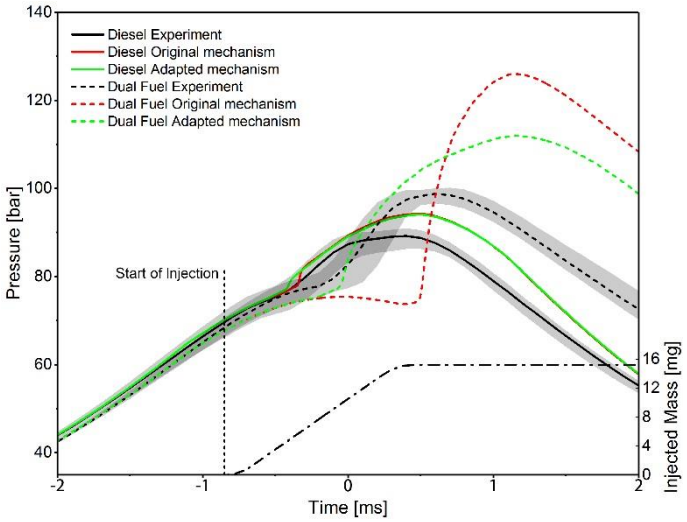

Figure 33. Pressure traces from the CFD simulation and measured values from a RCEM for diesel and dual fuel combustion with 20 % energetic diesel share using the mechanism before and after the optimization process. [20]

4.3 *Optimization of Kinetically Controlled Ignition Process*

To minimize the deviations between the experimental and CFD simulation values, the mechanism was adjusted to the RCEM and CV measurements, which resulted in a specific field of application for the mechanism. The mechanism was developed further to increase its applicability in a wider parameter range. Furthermore, the mechanism was not yet able to simulate the formation of nitrogen oxides (NO_x) during combustion, so a corresponding sub-mechanism was added. This advanced development process and mechanism adaptation is discussed in Paper III.

4.3.1 Re-Evaluation of Arrhenius Parameter Adjustments

To match the CFD simulation results to the experimentally determined values, reaction rate coefficients were changed, some greatly, lessening the potential applicability of the mechanism, as previously described. To obtain a larger application range, the further mechanism development investigated the kinetic-controlled ignition process. Therefore, the homogenous mixtures shown in Table 1 were studied to avoid a superposition of the actual ignition properties of the mixture and the influences of the inhomogeneous mixture preparation. With this objective in mind, the Arrhenius parameter changes made were reassessed and revised. Prior to this, the underlying San Diego base mechanism was updated, since a slightly changed mechanism version was released by the combustion research group at University of California San Diego that showed an increase in the number of reactions from 301 to 303. To calculate the NO_x formation during combustion, the San Diego nitrogen sub-mechanism was added. When revising the Arrhenius parameter adjustment, care was taken to ensure that the resulting reaction rate coefficient fell within the range of data collected from the literature in the NIST database.

4.3.2 Investigating the Influence of Propane Addition

The comparison between experiment and simulation of methane-propane mixtures (mixes 1 to 4 in Table 1) showed that the mechanism overestimated the IDT-reducing effect of propane, as can be seen on the right side of Figure 34. To determine which reactions could be used to reduce the overestimating behavior, a sensitivity analysis towards temperature was performed with mix 4 in Table 1. The temperature dependent course of the 10 most sensitive reactions can be seen on the left side of Figure 34.

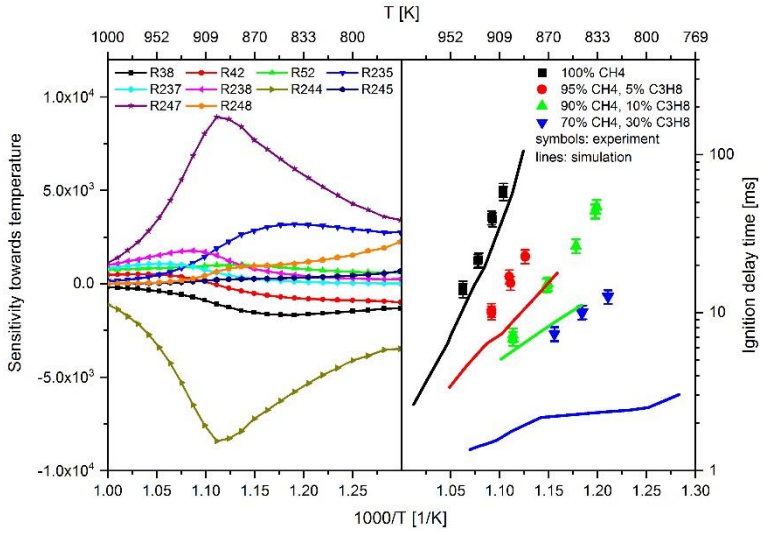

Figure 34. Sensitivity towards temperature simulated with mix 4 (left); measured IDTs (symbols) and simulated values (lines) for different methane-propane mixtures (right). The content of methane and propane is given in mol% and corresponds to mixes 1 to 4 in Table 1. [42]

In total, five reactions were used for the mechanism adjustment. An extract of the propane oxidation scheme derived from the mechanism is shown in Figure 35, with the reactions used for adaptation marked in red.

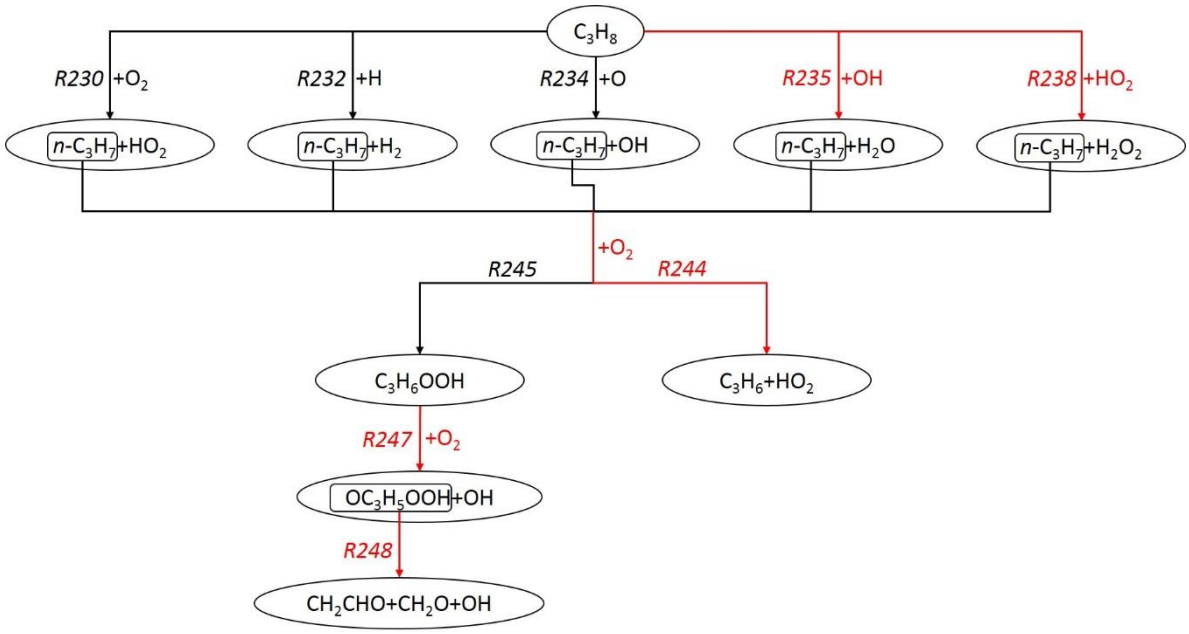

Figure 35. Extract from the propane oxidation scheme derived from the mechanism. Reactions with modified Arrhenius parameters to improve the calculation of the propane influence on the IDT are labeled in red. [42]

4.3.3 Laminar Flame Speed Calculation

To correctly reproduce the flame propagation after ignition in the combustion chamber of the dual fuel engine, the mechanism must allow the appropriate calculation of the laminar flame speed. To verify this, the simulated laminar flame speeds were compared with experimental values from the literature [53]. Since the background gas in the combustion chamber comprises a mixture of natural gas, which mostly consists of methane, and air, the laminar flame speed of methane-air mixtures was investigated. Flame speeds at 300 to 400 K, about 10 to 20 bar and fuel-air equivalence

ratios of 0.7 to 1.4 were studied. The comparison showed that the simulation underestimated the flame speed when the fuel-air equivalence ratio rose above 0.9. With the help of a sensitivity analysis, reactions with a high influence on the flame speed were identified. By adjusting the corresponding Arrhenius parameters, the deviation between simulation and experiment could be significantly reduced. As with all the adjustments made, reference data from the NIST database was used to justify the changes made.

4.3.4 Results of Mechanism Optimization

In total, 12 reactions were used to optimize the reaction mechanism regarding the reproduction of IDTs of homogenous mixtures and the laminar flame speed calculation. Table 2 provides an overview of the reactions used and each one's purpose in the adjustment of the corresponding Arrhenius parameters.

Table 2. Overview of the reactions used for the mechanism adaption and the purpose of the adaptation. [42]

Reaction number	Reaction equation	Purpose
42	$CH_4 + OH \leftrightarrow H_2O + CH_3$	Update of mechanism adjustments
44	$CH_4 + O_2 \leftrightarrow CH_3 + HO_2$	
45	$CH_4 + HO_2 \leftrightarrow CH_3 + H_2O_2$	
302	$n\text{-}C_7\text{-}OQOOH \leftrightarrow OH + CH_2O + CO + C_2H_4 + n\text{-}C_3H_7$	
235	$C_3H_8 + OH \leftrightarrow n\text{-}C_3H_7 + H_2O$	Correcting propane influence on IDT
238	$C_3H_8 + HO_2 \leftrightarrow n\text{-}C_3H_7 + H_2O_2$	
244	$n\text{-}C_3H_7 + O_2 \leftrightarrow C_3H_6 + HO_2$	
247	$C_3H_6OOH + O_2 \leftrightarrow OC_3H_5OOH + OH$	
248	$OC_3H_5OOH \leftrightarrow CH_2CHO + CH_2O + OH$	
1	$H + O_2 \leftrightarrow OH + O$	Correcting flame speed calculation
25	$CO + OH \leftrightarrow CO_2 + H$	
56	$CH_3 + H\ (+M) \leftrightarrow CH_4\ (+M)$	

The final parameter adjustment implemented, which led to the TU Wien dual fuel mechanism 2.0, was the adaptation of reactions 1, 25 and 56 in Table 2 to correct the laminar flame speed calculation. A comparison of the measured and calculated flame speed before and after the adjustment of the three reactions is presented in Figure 36.

Figure 37 shows a comparison of the experimentally determined IDTs and the simulation results using the mechanism based on the updated San Diego mechanism, including the parameter changes that were performed to reduce the deviations between the CFD simulations and experiments as described in section 4.2. Figure 37 includes this mechanism under the name of TU Wien dual fuel mechanism A. Furthermore, the simulation results using the mechanism that was optimized for the kinetically controlled ignition process (TU Wien dual fuel mechanism 2.0) are also shown for comparison.

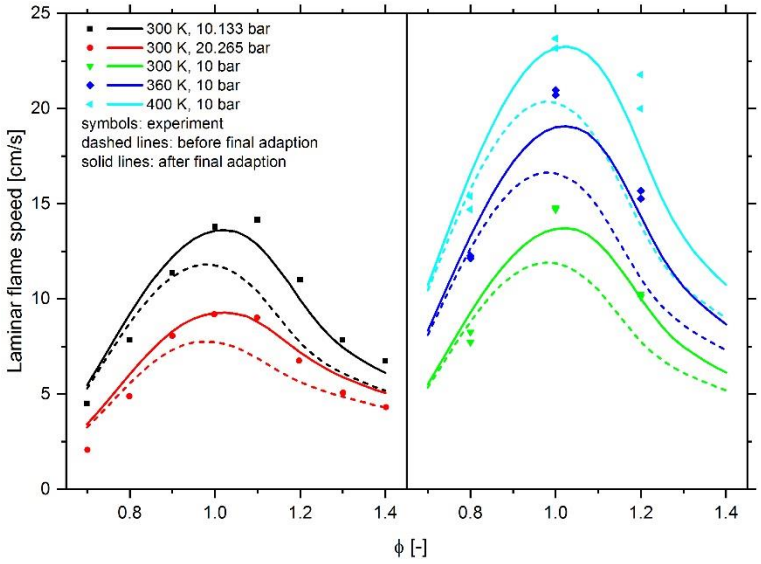

Figure 36. Measured laminar flame speeds of methane-air mixtures as function of the fuel-air equivalence ratio ϕ in comparison with simulated values before (dashed lines) and after the Arrhenius parameter adaption of reactions 1, 25, and 56 (solid lines). [42]

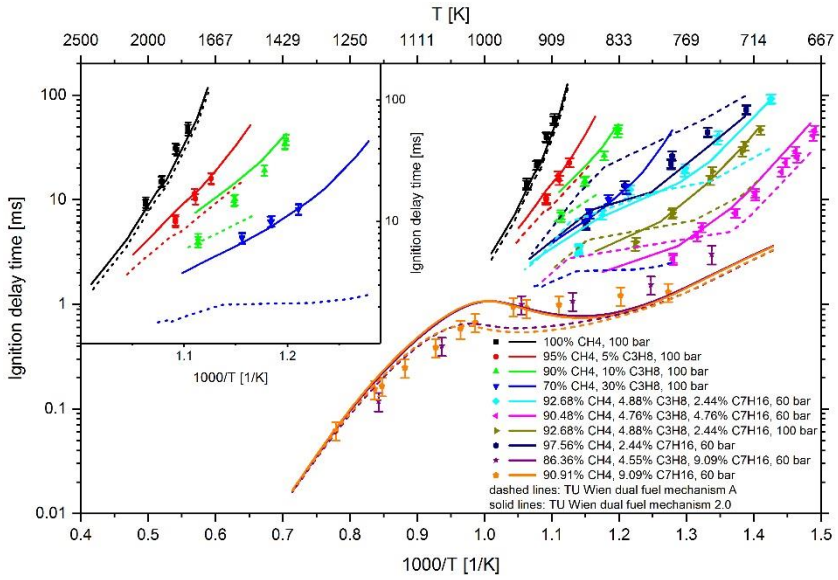

Figure 37. Experimental data (symbols) versus model prediction (lines) using the TU Wien dual fuel mechanism A (dashed lines) and the final TU Wien dual fuel mechanism 2.0 (solid lines). The diagram in the upper left corner highlights the difference between measured and calculated IDTs of methane-propane mixtures. The respective content of methane, propane, and *n*-heptane is given in mol% and corresponds to the values in Table 1. [42]

The TU Wien dual-fuel mechanism 2.0 was developed by modifying the 12 reactions listed in Table 2, which can successfully reproduce the IDT of the investigated homogeneous methane, methane-propane, methane-*n*-heptane, and methane-propane-*n*-heptane mixtures in the pressure range 60 to 100 bar. With measured values between 0.06 and 92 ms, IDTs over about three orders of magnitude are covered. Furthermore, the mechanism provides improved calculations of the laminar flame speed of methane-air mixtures.

5 Scientific Contribution of the Thesis

Nowadays, the use of simulations has proven indispensable in the development of modern combustion engines. To perform a temporally and spatially resolved computational fluid dynamics (CFD) engine simulation, precise knowledge of the internal processes in the engine is necessary. Detailed information on the chemical reactions occurring, the amounts of energy released in the processes and the correct calculation of the pressure as well as the temperature and velocity fields in the combustion chamber are all required to successfully reproduce fuel combustion by simulation. In the dual fuel combustion engine, two different fuels interact, which increases the complexity of the combustion process.

This thesis mainly aimed to analyze the dual fuel combustion process in detail and to develop a reaction mechanism to successfully simulate this process. Diesel and natural gas, as well as the diesel substitute *n*-heptane and the natural-gas substitute methane-propane mixture, were considered as fuels. In the investigations, various reaction mechanisms available in the literature were found to fail to accurately reproduce experimentally determined ignition properties. The mechanism that provided the most promising results was used as a basis for the new reaction mechanism to be developed. Sensitivity and flow analyses served to gain a detailed insight into the mechanism and to identify possibilities for the mechanism optimization. Ignition data of a rapid compression machine (RCM), shock tube (ST), rapid compression expansion machine (RCEM) and combustion vessel (CV) were used to evaluate the simulated ignition delay times (IDTs) of homogeneous and inhomogeneous mixtures. The homogeneous mixtures were investigated at very high pressure values of 60 to 100 bar, a fuel-air equivalence ratio between 0.526 and 0.816 and a temperature between 671 and 1284 K. Overall, experimentally determined ITDs that ranged almost three orders of magnitude, from 0.06 to 92 ms, were considered. In the study of inhomogeneous mixtures, the ignition processes of diesel injected in air (RCEM and CV tests) and a natural gas-air mixture (RCEM tests) were examined. The chamber pressure at the start of diesel injection in the RCEM was above 60 bar. Tests in the CV at a pressure of 60 bar were considered.

The TU Wien dual fuel reaction mechanism optimized for the RCEM- and CV-CFD simulations, consisting of 301 reactions and considering 64 species, successfully reproduced the IDTs measured in the RCEM, both in pure diesel operation and in dual fuel operation. Comparisons with measured values in the CV show a significant approximation of the simulated ITDs to the measured values in the temperature range between 923 and 973 K. The ignition characteristics of methane-propane mixtures can be correctly reproduced in a methane number (MN) range of 70 to 100.

When the reaction mechanism was further developed to yield a wider range of applications, the purely kinetic-controlled ignition process was considered by examining homogeneous mixtures. One major advantage of dual fuel operation over pure diesel operation lies in the significantly reduced nitrogen oxides (NO_x) emissions. To calculate the formation of NO_x during combustion, the reaction mechanism was extended to include 344 reactions and consider 75 species. The ongoing development process of the mechanism aimed to improve the calculation of methane-propane mixture ignition properties. The MN range with satisfactory IDT calculation from 70 to 100 could be extended to the entire experimentally investigated MN range of 50 to 100. This thesis also examined the simulation of flame propagation in the background gas of the combustion chamber. Experimentally determined flame speeds, drawn from the literature, at pressures of about 10 to 20 bar, temperatures between 300 and 400 K and a fuel-air equivalence ratio of 0.7 to 1.4 of methane-air mixtures allowed the evaluation of the simulated values. By means of sensitivity analyses, influential reactions were identified and used to optimize the mechanism. By adapting the mechanism, the flame speed could be reproduced well over the mentioned parameter range. In addition to the amended calculation of the methane-propane mixture ignition properties, the TU Wien dual fuel mechanism 2.0 showed an improved reproduction of the measured values from the investigated methane-*n*-heptane and methane-propane-*n*-heptane mixtures, thus surpassing all previous results of the mechanisms from various literature sources investigated within the scope of the thesis.

The developed reaction mechanisms offer the scientific community new possibilities for more detailed research in the field of dual fuel combustion.

6 References

1. Karim, G.A. *Dual-fuel diesel engines*; Boca Raton : CRC Press, Taylor & Francis Group: Boca Raton, 2015; pp. 1 Online-Ressource, illustrations.
2. Ohashi, I. Dual-Fuel Marine Engine (Highly Reliable Environmentally Friendly Engine). Availabe online: https://www.yanmar.com/global/technology/technical_review/2015/0727_2.html (accessed on 14 Januar 2020).
3. Crude Oil Prices - 70 Year Historical Chart. Availabe online: https://www.macrotrends.net/1369/crude-oil-price-history-chart (accessed on 21 February 2020).
4. Paris Agreement. Availabe online: https://ec.europa.eu/clima/policies/international/negotiations/paris_en (accessed on 20 November 2019).
5. Winkel, R.; Weddige, U.; Johnsen, D.; Hoen, V.; Papaefthimiou, S. Shore Side Electricity in Europe: Potential and environmental benefits. *Energy Policy* **2016**, *88*, 584-593, doi:10.1016/j.enpol.2015.07.013.
6. World Health Organization. Regional Office for, E. Health aspects of air pollution with particulate matter, ozone and nitrogen dioxide: report on a WHO working group, Bonn, Germany 13-15 January 2003. Copenhagen : WHO Regional Office for Europe: 2003.
7. Nitrogen Oxides (NOx) – Regulation 13 Availabe online: http://www.imo.org/en/OurWork/Environment/PollutionPrevention/AirPollution/Pages/Nitrogen-oxides-(NOx)-%E2%80%93-Regulation-13.aspx (accessed on 14 January 2020).
8. Transport von Gütern auf der Straße. Availabe online: https://www.umweltbundesamt.at/umweltsituation/verkehr/fahrzeugtechnik/lkw/ (accessed on 16 January 2020).
9. Schlick, H. Potentials and challenges of gas and dual-fuel engines for marine application [Presentation]. In Proceedings of 5th CIMAC CASCADES, Busan, South Korea, 2014.
10. Understanding Global Warming Potentials. Availabe online: https://www.epa.gov/ghgemissions/understanding-global-warming-potentials (accessed on 9 December 2019).
11. Chemical-Kinetic Mechanisms for Combustion Applications; San Diego Mechanism Web Page, Mechanical and Aerospace Engineering (Combustion Research), University of California at San Diego. Availabe online: http://combustion.ucsd.edu (accessed on 4 October 2019).
12. Fischer, M. *Modellierung der Multikomponenten-Verdampfung im homogenisierten dieselmotorischen Brennverfahren*; Cuvillier Verlag Göttingen: 2006; Vol. 1.
13. Joos, F. *Technische Verbrennung*; Berlin [u.a.]: Springer: Berlin [u.a.], 2006; 10.1007/3-540-34334-2.
14. van Basshuysen, R. *Erdgas und erneuerbares Methan für den Fahrzeugantrieb: Wege zur klimaneutralen Mobilität*; Springer Fachmedien Wiesbaden, Wiesbaden: Wiesbaden, 2015; 10.1007/978-3-658-07159-2.
15. Al-Saleh, M.A.; Duffuaa, S.O.; Al-Marhoun, M.A.; Al-Zayer, J.A. Impact of crude oil production on the petrochemical industry in Saudi Arabia. *Energy* **1991**, *16*, 1089-1099, doi:10.1016/0360-5442(91)90141-8.
16. Mollenhauer, K.; Tschöke, H. *Handbuch Dieselmotoren*, 3., neubearbeitete Auflage. ed.; Berlin, Heidelberg : Springer-Verlag Berlin Heidelberg: Berlin, Heidelberg, 2007; 10.1007/978-3-540-72165-9.
17. Karavalakis, G.; Hajbabaei, M.; Durbin, T.D.; Johnson, K.C.; Zheng, Z.; Miller, W.J. The effect of natural gas composition on the regulated emissions, gaseous toxic pollutants, and ultrafine particle number emissions from a refuse hauler vehicle. *Energy* **2013**, *50*, 280-291, doi:10.1016/j.energy.2012.10.044.

18. Kidnay, A.J.; Parrish, W.R. *Fundamentals of Natural Gas Processing*; CRC Press: Boca Raton, FL, USA, 2006.
19. Cummins Westport Fuel Quality Calculator. Availabe online: https://www.cumminswestport.com/fuel-quality-calculator (accessed on 12.11.2019).
20. Schuh, S.; Frühhaber, J.; Lauer, T.; Winter, F. A Novel Dual Fuel Reaction Mechanism for Ignition in Natural Gas–Diesel Combustion. *Energies* **2019**, *12*, doi:10.3390/en12224396.
21. Szymkowicz, P.G.; Benajes, J. Development of a Diesel Surrogate Fuel Library. *Fuel* **2018**, *222*, 21-34, doi:10.1016/j.fuel.2018.01.112.
22. Eder, L.; Ban, M.; Pirker, G.; Vujanovic, M.; Priesching, P.; Wimmer, A. Development and Validation of 3D-CFD Injection and Combustion Models for Dual Fuel Combustion in Diesel Ignited Large Gas Engines. *Energies* **2018**, *11*, doi:10.3390/en11030643.
23. Ritzke, J.; Andree, S.; Theile, M.; Henke, B.; Schleef, K.; Nocke, J.; Hassel, E. Simulation of a Dual-Fuel Large Marine Engines using combined 0/1-D and 3-D Approaches. In Proceedings of CIMAC Congress, Helsinki, Finland, 2016.
24. Li, Y.; Li, H.; Guo, H.; Li, Y.; Yao, M. A numerical investigation on methane combustion and emissions from a natural gas-diesel dual fuel engine using CFD model. *Applied Energy* **2017**, *205*, 153-162, doi:10.1016/j.apenergy.2017.07.071.
25. Tschöke, H. *Diesel- und Benzindirekteinspritzung V: Spraybildung, Simulation, Applikation, Messtechnik : mit 29 Tabellen*; expert-Verlag: 2009.
26. Reif, K. *Dieselmotor-Management: Systeme, Komponenten, Steuerung und Regelung*; Vieweg+Teubner Verlag: Wiesbaden, Germany, 2012.
27. Riess, S.; Weiss, L.; Peter, A.; Rezaei, J.; Wensing, M. Air entrainment and mixture distribution in Diesel sprays investigated by optical measurement techniques. *International Journal of Engine Research* **2017**, *19*, 120-133, doi:10.1177/1468087417742527.
28. Kim, S.; Chen, J.; Cheng, T.; Gindulyte, A.; He, J.; He, S.; Li, Q.; Shoemaker, B.A.; Thiessen, P.A.; Yu, B., et al. PubChem 2019 update: improved access to chemical data. *Nucleic Acids Research* **2018**, *47*, D1102-D1109, doi:10.1093/nar/gky1033.
29. Warnatz, J. *Verbrennung : physikalisch-chemische Grundlagen, Modellierung und Simulation, Experimente, Schadstoffentstehung*, 2., überarb. und erw. Aufl. ed.; Berlin [u.a.] : Springer: Berlin [u.a.], 1997; pp. X, 277 S., Ill., zahlr. graph. Darst.
30. Günter, P.M.; Rüdiger, T. *Grundlagen Verbrennungsmotoren: Funktionsweise, Simulation, Messtechnik*; Springer Fachmedien Wiesbaden, Wiesbaden: Wiesbaden, 2014; 10.1007/978-3-658-03195-4.
31. Schuh, S.; Ramalingam, A.K.; Minwegen, H.; Heufer, K.A.; Winter, F. Experimental Investigation and Benchmark Study of Oxidation of Methane–Propane–n-Heptane Mixtures at Pressures up to 100 bar. *Energies* **2019**, *12*, doi:10.3390/en12183410.
32. Pachler, R.F.; Ramalingam, A.K.; Heufer, K.A.; Winter, F. Reduction and validation of a chemical kinetic mechanism including necessity analysis and investigation of CH4/C3H8 oxidation at pressures up to 120 bar using a rapid compression machine. *Fuel* **2016**, *172*, 139-145, doi:10.1016/j.fuel.2015.12.044.
33. Petersen, E.L.; Hanson, R.K. Nonideal effects behind reflected shock waves in a high-pressure shock tube. *Shock Waves* **2001**, *10*, 405-420, doi:10.1007/pl00004051.
34. Heufer, K.A.; Olivier, H. Determination of ignition delay times of different hydrocarbons in a new high pressure shock tube. *Shock Waves* **2010**, *20*, 307-316, doi:10.1007/s00193-010-0262-2.
35. Frühhaber, J.; Peter, A.; Schuh, S.; Lauer, T.; Wensing, M.; Winter, F.; Priesching, P.; Pachler, K. Modeling the Pilot Injection and the Ignition Process of a Dual Fuel Injector with Experimental Data

from a Combustion Chamber Using Detailed Reaction Kinetics. **2018**, *SAE Technical Paper 2018-01-1724*, doi:10.4271/2018-01-1724.

36. Peter, A.; Frühhaber, J.; Schuh, S.; Lauer, T.; Winter, F.; Priesching, P.; Wensing, M. Flame quenching during dual-fuel operation investigated in experiments and simulation. In Proceedings of THIESEL 2018 Conference on Thermo- and Fluid Dynamic Processes in Direct Injection Engines, Valencia, Spain, 2018.
37. Kee, R.J.; Rupley, F.M.; Miller, J.A.; Coltrin, M.E.; Grcar, J.F.; Meeks, E.; Moffat, H.K.; Lutz, A.E.; Dixon-Lewis, G.; Smooke, M.D., et al. CHEMKIN Collection, Release 3.6, Reaction Design. *Inc., San Diego, CA, USA* **2000**.
38. Soyhan, H.S.; Mauss, F.; Sorusbay, C. Chemical kinetic modeling of combustion in internal combustion engines using reduced chemistry. *Combustion Science and Technology* **2002**, *174*, 73-91, doi:10.1080/713712950.
39. LOGEresearch. Availabe online: https://logesoft.com/loge-software/ (accessed on 16 May 2019).
40. Soyhan, H.; Amnéus, P.; Mauss, F.; Sorusbay, C. A Skeletal Kinetic Mechanism for the Oxidation of iso-Octane and n-Heptane Validated under Engine Knock Conditions. **1999**, *SAE Technical Paper 1999-01-3484*, doi:10.4271/1999-01-3484.
41. Ji, W.; Ren, Z.; Law, C.K. Evolution of sensitivity directions during autoignition. *Proceedings of the Combustion Institute* **2019**, *37*, 807-815, doi:10.1016/j.proci.2018.07.005.
42. Schuh; Winter. Dual Fuel Reaction Mechanism 2.0 including NOx Formation and Laminar Flame Speed Calculations Using Methane/Propane/n-Heptane Fuel Blends. *Energies* **2020**, *13*, doi:10.3390/en13040778.
43. Lennartz, Y. Ottomotoren - Ottomotorische Verbrennung. Availabe online: http://www.sfb224.rwth-aachen.de/Kapitel/kap3_3.htm (accessed on 20 February 2020).
44. Kammerdiener, T.; Schlick, H.; Hirschl, G.; Zallinger, M.; Schönbacher, M. Konzeptuntersuchungen für einen Dual Fuel Motor basierend auf Versuchen an einem schnelllaufenden Einzylindermotor. In Proceedings of 9th Dessau Gas Engine Conference, Dessau, Germany, 2015.
45. Huang, H.; Lv, D.; Zhu, J.; Zhu, Z.; Chen, Y.; Pan, Y.; Pan, M. Development of a new reduced diesel/natural gas mechanism for dual-fuel engine combustion and emission prediction. *Fuel* **2019**, *236*, 30-42, doi:10.1016/j.fuel.2018.08.161.
46. Cai, L.; Pitsch, H. Optimized chemical mechanism for combustion of gasoline surrogate fuels. *Combustion and Flame* **2015**, *162*, 1623-1637, doi:10.1016/j.combustflame.2014.11.018.
47. Mehl, M.; Pitz, W.J.; Westbrook, C.K.; Curran, H.J. Kinetic modeling of gasoline surrogate components and mixtures under engine conditions. *Proceedings of the Combustion Institute* **2011**, *33*, 193-200, doi:10.1016/j.proci.2010.05.027.
48. Zhang, K.; Banyon, C.; Bugler, J.; Curran, H.J.; Rodriguez, A.; Herbinet, O.; Battin-Leclerc, F.; B'Chir, C.; Heufer, K.A. An updated experimental and kinetic modeling study of n-heptane oxidation. *Combustion and Flame* **2016**, *172*, 116-135, doi:10.1016/j.combustflame.2016.06.028.
49. Metcalfe, W.K.; Burke, S.M.; Ahmed, S.S.; Curran, H.J. A Hierarchical and Comparative Kinetic Modeling Study of C1−C2 Hydrocarbon and Oxygenated Fuels. *International Journal of Chemical Kinetics* **2013**, *45*, 638-675, doi:10.1002/kin.20802.
50. Li, Y.; Zhou, C.-W.; Somers, K.P.; Zhang, K.; Curran, H.J. The oxidation of 2-butene: A high pressure ignition delay, kinetic modeling study and reactivity comparison with isobutene and 1-butene. *Proceedings of the Combustion Institute* **2017**, *36*, 403-411, doi:10.1016/j.proci.2016.05.052.

51. Zhou, C.-W.; Li, Y.; Burke, U.; Banyon, C.; Somers, K.P.; Ding, S.; Khan, S.; Hargis, J.W.; Sikes, T.; Mathieu, O., et al. An experimental and chemical kinetic modeling study of 1,3-butadiene combustion: Ignition delay time and laminar flame speed measurements. *Combustion and Flame* **2018**, *197*, 423-438, doi:10.1016/j.combustflame.2018.08.006.

52. Manion, J.A.; Huie, R.E.; Levin, R.D.; Jr., D.R.B.; Orkin, V.L.; Tsang, W.; McGivern, W.S.; Hudgens, J.W.; Knyazev, V.D.; Atkinson, D.B., et al. NIST Chemical Kinetics Database, NIST Standard Reference Database 17, Version 7.0 (Web Version), Data version 2015.09. National Institute of Standards and Technology, Gaithersburg, Maryland.

53. Ranzi, E.; Frassoldati, A.; Grana, R.; Cuoci, A.; Faravelli, T.; Kelley, A.P.; Law, C.K. Hierarchical and comparative kinetic modeling of laminar flame speeds of hydrocarbon and oxygenated fuels. *Progress in Energy and Combustion Science* **2012**, *38*, 468-501, doi:10.1016/j.pecs.2012.03.004.

7 Appendix (Journal Paper I, II and III, Curriculum Vitae)